

The Design of Salinity Sensor for Antarctic Research



Prepared by:

Cameron Clark

Department of Electrical Engineering
University of Cape Town

Prepared for:

Justin Pead

Department of Electrical Engineering
University of Cape Town

October 24, 2024

Submitted to the Department of Electrical Engineering at the University of Cape Town in partial fulfilment of the academic requirements for a Bachelor of Science degree in Mechatronics

Keywords: Salinity, Sensor, Conductivity, Temperature, Water, Measurement, Electronics, PCB

Declaration

1. I know that plagiarism is wrong. Plagiarism is to use another's work and pretend that it is one's own.
2. I have used the IEEE convention for citation and referencing. Each contribution to, and quotation in, this report from the work(s) of other people has been attributed and has been cited and referenced. Any section taken from an internet source has been referenced to that source.
3. This report is my own work and is in my own words (except where I have attributed it to others).
4. I have not paid a third party to complete my work on my behalf. My use of artificial intelligence software has been limited to (specify precisely how you used AI to assist with this assignment, and then give examples of the prompts you used in your first appendix).
5. I have not allowed and will not allow anyone to copy my work with the intention of passing it off as his or her own work.
6. I acknowledge that copying someone else's assignment or essay, or part of it, is wrong, and declare that this is my own work



October 24, 2024

Cameron Clark

Date

Acknowledgements

Abstract

Contents

List of Figures	vi
Abbreviations	vii
1 Introduction	1
1.1 Problem Statement	1
1.2 Background	1
1.3 Objectives	2
1.4 Scope & Limitations	2
1.5 Report Outline	2
2 Literature Review	3
2.1 Introduction	3
2.2 Salinity Definitions	3
2.3 The Uses of Salinity Measurements	4
2.4 Salinity Measurement Methods	4
2.4.1 Salinity from Chlorinity	4
2.4.2 Salinity from Conductivity	5
2.4.3 Salinity from Density	5
2.4.4 Salinity from Microwave Radiation	5
2.4.5 Salinity from Refractive Index	6
2.4.6 Salinity from Interferometry	6
2.4.7 Salinity from Magnetic Permeability	7
2.5 Salinity Measurement Devices using Conductivity	7
3 Theory Development	9
3.1 The Calculation of Salinity From Conductivity	9
3.2 Salt water's Resistance-Voltage Measurement	11
3.3 Current Fringing in Conductive Materials	11
4 Design	12
4.1 Salinity Measurement Method	12
4.2 Conductivity Electrode Material	12
4.3 Conductivity Electrode Design	13
4.4 Resistance Measurement Method	15
4.5 Circuit Overview	15
4.6 Salinity Calculation and Display	18
4.7 Temperature and Depth Measurement	18

5 PCB Construction, Adjustments and Code	20
5.1 PCB Design	20
5.2 PCB Adjustments	21
5.3 Probe Code	22
5.4 Controller Code	23
5.5 Board-to-Board Communication	24
5.6 Probe Epoxy Casting	25
6 Salinometer Evaluation and Testing	27
6.1 Overview	27
6.2 Testing Apparatus	28
6.3 DAC Voltage Range and Accuracy	28
6.4 ADC Accuracy	29
6.5 Calibration Resistance	30
6.6 Resistance Measuring Accuracy	30
6.7 Voltage Sweep Repeatability	31
6.8 Voltage to Conductivity Mapping	34
6.9 Individual Voltage Measurements	37
6.10 AC Voltage Measurements	37
7 Conclusions	39
8 Recommendations	40
Bibliography	41

List of Figures

2.1	Global salinity map generated using satellite data [25].	6
2.2	The schematic of a Conductivity, Temperature, Depth (CTD) probe developed by researchers at Uppsala University in Sweden which design contains (a) a temperature sensor, (b) three relatively small electrodes for pH and Cl- concentration, (c) conductivity electrodes, and (d) a strain gauge for the pressure membrane sensor. The design is $7.5 \times 3.5\text{mm}$ in size [40].	8
4.1	The gold electrode Printed Circuit Board (PCB) design.	14
4.2	A simplified representation of the resistance measuring circuit.	16
4.3	A simplified representation of the resistance measurement circuit using the gold electrodes with the fringe guard.	17
5.1	The probe PCB with the gold electrodes attached and some adjustments made	20
5.2	The controller PCB with the rotary switch caps attached	21
5.3	The flowchart for the probe code that measures salinity.	23
5.4	The flowchart for the board-to-board communication protocol denoting the four transaction types. The arrows denote the direction of the packets being sent over the Recommended Standard #485 (RS-485) link.	24
5.5	A top view of the probe casting mould, the controller and the connecting cable.	25
5.6	A side view of the probe casting mould showing the gold electrode spacers.	25
5.7	The probe after the epoxy casting process with the titanium electrodes and pressure sensor's flexible membrane attached.	26
5.8	A close-up of the titanium electrode with the copper wire attached.	26
6.1	The salinometer probe with multimeter cables attached to a test point and ground.	28
6.2	The bench multimeter used for the tests displaying a voltage reading.	28
6.3	The input voltage versus the output voltage of the Digital to Analogue Converter (DAC) with no load.	29
6.4	The input voltage versus the output voltage of the DAC with the maximum load of 100Ω	29
6.5	The voltage output by the DAC measured by a multimeter versus by the Analogue to Digital Converter (ADC).	29
6.6	The resistance measuring test.	30
6.7	The resistance measuring test using the corrected equation.	30
6.8	Conductivity test 1 with gold electrodes and the fringe shield, a voltage range of $0-2,6V$, and 50 samples taken of salt water sample of unknown salinity.	32
6.9	Conductivity test 2 with draining and resetting the DAC between each voltage sample.	32
6.10	Conductivity test 3 with 25 priming measurements taken before the actual measurement.	33

6.11 Conductivity test 4 with a varying number of priming measurements and all true measurement taken as reverse voltage sweeps with 500 voltage samples.	33
6.12 Conductivity test 5 with a varying amount of relaxation time before each measurement was taken and 50 samples.	33
6.13 Conductivity test 6 with the difference between the titanium and gold electrodes.	33
6.14 Conductivity test 7 with 4 identical tests of 20 samples with 2s of relaxation time between measurements.	34
6.15 Conductivity test 6 with 4 identical tests of 20 samples with 2s of relaxation time between measurements.	34
6.16 Conductivity test 6 with 4 identical tests of 20 samples with 2s of relaxation time between measurements.	35
6.17 Conductivity test 7 with 4 identical tests of 20 samples with 2s of relaxation time between measurements.	35
6.18 Conductivity test 6 with 4 identical tests of 20 samples with 2s of relaxation time between measurements.	36
6.19 Conductivity test 7 with 4 identical tests of 20 samples with 2s of relaxation time between measurements.	36
6.20 Conductivity test 6 with 4 identical tests of 20 samples with 2s of relaxation time between measurements.	36
6.21 Conductivity test 7 with 4 identical tests of 20 samples with 2s of relaxation time between measurements.	36
6.22 Conductivity test 6 with 4 identical tests of 20 samples with 2s of relaxation time between measurements.	37
6.23 Conductivity test 7 with 4 identical tests of 20 samples with 2s of relaxation time between measurements.	37
6.24 Conductivity test 6 with 4 identical tests of 20 samples with 2s of relaxation time between measurements.	38
6.25 Conductivity test 7 with 4 identical tests of 20 samples with 2s of relaxation time between measurements.	38
6.26 Conductivity test 6 with 4 identical tests of 20 samples with 2s of relaxation time between measurements.	38
6.27 Conductivity test 7 with 4 identical tests of 20 samples with 2s of relaxation time between measurements.	38

Abbreviations

%o Parts Per Thousand

AC Alternating Current

ADC Analogue to Digital Converter

CTD Conductivity, Temperature, Depth

DAC Digital to Analogue Converter

DMA Direct Memory Access

EMI Electromagnetic Interference

ENIG Electroless Nickel Immersion Gold

FPU Floating Point Unit

IC Integrated Circuit

LCR Inductance (L), Capacitance (C), Resistance (R)

LED Light Emitting Diode

PCB Printed Circuit Board

ppm parts per million

PSU Practical Salinity Units

RS-485 Recommended Standard #485

SCB System Control Block

SST Sea Surface Temperature

SYSRESETREQ System Reset Request

UART Universal Asynchronous Receiver-Transmitter

UCT University of Cape Town

USB Universal Serial Bus

Chapter 1

Introduction

1.1 Problem Statement

There are several methods and designs for measuring salinity which is commonly understood as the salt content of water. However, Antarctica's freezing temperatures and harsh conditions make it challenging for scientists to study this metric there. The current method of measuring involves capturing a water sample from the ocean beneath the ice sheet and bringing it to the surface for measurement. This process alters some water's physical properties, such as temperature and pressure, which can affect the salinity measurement. This project aims to design a device that can more accurately measure the salinity by using a probe to take measurements at various depths in the ocean.

1.2 Background

Antarctica is covered in a vast sheet of ice consisting of around 30 million cubic kilometres in volume, which is about 60% of the world's fresh water [1]. Part of the ice sheets rests on land, known as the continental ice sheet, while the rest floats on the ocean, known as the ice shelves [2]. The ice sheet supports a variety of species both above and below it, as well as an ecosystem within the ice itself [3].

The ice shelves surrounding the Antarctic continent constantly wax and wane [4], with the ice thickening during winter with water and salt accumulating from precipitation, sea spray, and ocean water freezing in direct contact with the ice [5]. When the water freezes, the salts are expelled from the mixture, creating small pockets and highly saline water channels known as brine channels. The brine channels form a habitat for several microorganisms that have adapted to the cold, harsh environment and a new habitat when they drain into the ocean below. Frigid brine and regular seawater mix beneath the ice shelves, creating a mixing zone which forms a unique environment that supports life. Scientists working with the [University of Cape Town \(UCT\)](#) are currently investigating the properties of the mixing zone, such as the water's salinity, temperature, currents, light penetration, and more.

To measure any given property, an ice core is drilled through the ice shelf down to the water's surface, and two main methods are employed to measure the brine-sea water mixture. Either a probe is lowered into the water through the ice core hole, allowing measurements to be taken at multiple depths, or a sample of the water is captured by lowering an open canister known as a Niskin bottle into the water, closing it at the desired depth, and retrieving it for analysis with hand-held instruments. Salinity is currently being measured using the latter method, which could be improved as the water sample changes temperature and pressure as it is brought to the surface, which can affect the salinity

measurement.

1.3 Objectives

The objectives of this project are to design and develop a prototype device for measuring the salinity of the water beneath the ice shelf. The prototype should aid in investigating its feasibility and understanding the methodology for measuring salinity. It should set the foundation for a future device to be developed that can be used in the field. The final device should be able to withstand Antarctica's harsh temperatures and conditions, but these will only be secondary considerations in this project.

1.4 Scope & Limitations

This project's scope includes the design and development of a prototype device for measuring salinity. This includes researching the relevant literature that details devices with similar functionality, the theory behind measuring salinity, followed by the design and development of a prototype device that can test the properties of salt water and lead to a method of measuring salinity. The prototype development involves testing and evaluating the device to determine its effectiveness in measuring salinity. Additionally, this project should aim to develop the prototype as a separate probe and control unit. The scope does not extend to any development for the final device beyond the prototype nor the analysis of any data captured should the prototype be used in the field.

This project has a budget limitation of R2000 for the entire design, development and testing. This budget can only be spent through [UCT](#) with their approved suppliers and vendors. The project must be completed in 14 weeks from the start to the submission of the final report.

1.5 Report Outline

 Lorem ipsum dolor sit amet, consectetuer adipiscing elit. Ut purus elit, vestibulum ut, placerat ac, adipiscing vitae, felis. Curabitur dictum gravida mauris. Nam arcu libero, nonummy eget, consectetuer id, vulputate a, magna. Donec vehicula augue eu neque. Pellentesque habitant morbi tristique senectus et netus et malesuada fames ac turpis egestas. Mauris ut leo. Cras viverra metus rhoncus sem. Nulla et lectus vestibulum urna fringilla ultrices. Phasellus eu tellus sit amet tortor gravida placerat. Integer sapien est, iaculis in, pretium quis, viverra ac, nunc. Praesent eget sem vel leo ultrices bibendum. Aenean faucibus. Morbi dolor nulla, malesuada eu, pulvinar at, mollis ac, nulla. Curabitur auctor semper nulla. Donec varius orci eget risus. Duis nibh mi, congue eu, accumsan eleifend, sagittis quis, diam. Duis eget orci sit amet orci dignissim rutrum.

Chapter 2

Literature Review

2.1 Introduction

This literature review starts with introducing the concept of salinity and its history. It then discusses the importance and various uses of salinity measurements. The review then covers the various documented methods of measuring salinity, followed by a review of the devices that used conductivity to measure salinity, which is the industry standard. The review concludes with the theory and calculation of salinity from conductivity measurements.

2.2 Salinity Definitions

The most commonly understood definition of salinity relates to the total amount of dissolved *salts* in a solution. However, salinity's definition has had several more complex iterations over the last century. One of the first definitions of salinity was the total amount of dissolved *material* in grams in one kilogram of water [6], which is a dimensionless quantity that was expressed in [Parts Per Thousand \(%\)](#) or $g.kg^{-1}$ where most of the ocean water's salinity falls between 34.60% and 34.80% [6].

The problem with this definition lies in its testability. Trying to obtain the mass of the dissolved material through evaporation removed certain compounds, making this method inaccurate [7] and other methods of isolating the mass of the dissolved material had similar issues [6]. The need for testability led to salinity being redefined in 1969 to be related to the amount of chlorine present in the water, better known as chlorinity [6]. Chlorinity measurements were well established, and the salinity calculation from chlorinity was relatively simple, which is further discussed in [Section 2.4.1](#).

Around the same time as the salinity-chlorinity relationship was established, oceanographers began experimenting with using conductivity to measure salinity. Conductivity was more precise and straightforward than the titration required to measure chlorinity [8]. In 1978, the Practical Salinity Scale was established, which defined salinity in terms of conductivity and is regarded as the current definition of salinity [8]. While the conductivity measurement was considered easy, the salinity-conductivity relationship was more complex as it had to include corrections for temperature and depth as they both affect the conductivity of an electrolyte solution [9].

The Practical Salinity Scale uses dimensionless units of salinity, which are approximately equivalent to [Parts Per Thousand \(%\)](#) [10] in the current definition of salinity [11]. Although the Practical Salinity Scale is sometimes given in [Practical Salinity Units \(PSU\)](#), it is more technically correct to refer to

it as a certain Practical Salinity ‘on the Practical Salinity Scale PSS-78’ [8]. The salinity calculation from conductivity is further discussed in Section 3.1.

2.3 The Uses of Salinity Measurements

2.4 Salinity Measurement Methods

Salinity has had a long history of being measured using various methods with varying degrees of accuracy. Currently, the most common method of measuring salinity is using a [Conductivity, Temperature, Depth \(CTD\)](#) instrument. However, there are multiple alternative methods, most of which have been developed over the last three decades, a summary of which is provided in Table 2.1.

Table 2.1: Summary of the various methods of measuring salinity.

Method	Key Advantages	Key Disadvantages	Highest Accuracy
Chlorinity	<ul style="list-style-type: none"> Concisely defined Well established 	<ul style="list-style-type: none"> Requires titration Has human error 	0.01‰ [7]
Conductivity	<ul style="list-style-type: none"> Industry standard Automated devices available 	<ul style="list-style-type: none"> Complex relationship Requires temperature and depth corrections 	0.0002 PSU [12]
Density	<ul style="list-style-type: none"> Accounts for all dissolved material 	<ul style="list-style-type: none"> Complex relationship Requires temperature correction 	0.003 PSU [13]
Microwave Radiation	<ul style="list-style-type: none"> Measurable from a distance including from space 	<ul style="list-style-type: none"> Requires many corrections Expensive instrument 	0.1 PSU [14]
Refractive Index	<ul style="list-style-type: none"> Compact devices available 	<ul style="list-style-type: none"> Complex relationship Requires temperature and pressure corrections 	0.4‰ [15]
Interferometry	<ul style="list-style-type: none"> High accuracy reported 	<ul style="list-style-type: none"> Large, complex instrument Difficult to implement 	0.001 PSU [16]
Electromagnetic Induction	<ul style="list-style-type: none"> Non-destructive 	<ul style="list-style-type: none"> Not well researched Large, high power instrument 	-

2.4.1 Salinity from Chlorinity

The chemical composition of ocean water with a salinity of 35‰ contains 19.35‰ of Chlorine and 10.77‰ of Sodium with the following most common ions only accounting for just above 3‰ of the total dissolved solids in the water [17]. This allowed oceanographers to determine that the salinity of ocean water was directly proportional to the amount of chlorine in the water, which holds true provided

the ratios of the dissolved materials in the water remained constant. The chlorinity of a solution has an established definition, which is ‘the mass of silver required to precipitate completely the halogens in 0.328 523 4kg of the ocean-water sample’ [18] which could be tested using titration. In 1969, an accurate relationship between these was established by Reference [18], shown in Equation 2.1, which was significantly more accurate than the evaporation method achieving accuracies within 0.01‰ [7] but was still limited by human error [8].

$$S(\%) = 1.80655 \times Cl(\%) \quad (2.1)$$

2.4.2 Salinity from Conductivity

The conductivity of a liquid is a measure its ability to conduct electrical current, which is related to the number of free electrons present in the liquid, which is in turn related to the number of ions present in the liquid [6]. In the case of salt water, the ions present are from the dissolved material, which salinity was previously defined on [6]. The relationship between salinity and conductivity accounts for all the ions in the water as opposed to just chlorine which is why it was considered a more apt measure of salinity [8]. Measuring conductivity was more accurate than titration, achieving accuracies within 0.0002 on the Practical Salinity Scale PSS-78 [12]. The conductivity measurement is typically done using a CTD which measures the conductivity as well as the temperature and depth that are required to accurately calculate salinity. CTD devices are discussed further in Section 2.5 and the calculation of salinity from conductivity is further discussed in Section 3.1.

2.4.3 Salinity from Density

The density of pure water varies with temperature and is approximately 1000kg.m^{-3} at 4°C [19]. Adding denser materials to the water will intuitively increase its density. This concept is used to determine the quantity of added material using a density measurement, which can be used to calculate salinity [20]. The relationship between salinity and density is approximately linear as shown in Equation 2.2 where ρ is the density of the water, ρ_0 is the density of pure water, k is a proportionality constant, and S is the salinity of the water [21].

$$\rho = \rho_0(1 + kS) \quad (2.2)$$

The more accurate relationship is more complicated and includes a temperature correction defined by Reference [13]. While the accuracy of salinity from density was less than that from conductivity with accuracies within 0.003 on the Practical Salinity Scale PSS-78 [13], Reference [22] still claimed that density was more appropriate to use as the standard potassium chloride solution used to calibrate the CTDs meters did not account for the variation of the ratios of conductive and non-conductive materials commonly present in salt water while the density of the water did.

2.4.4 Salinity from Microwave Radiation

The electromagnetic spectrum interacts uniquely with salt water, scattering, refracting, and reflecting when in contact with it or any material dissolved in it. Different temperature molecules in the water interact with electromagnetic waves differently, and the pressure of the water also varies this interaction.

However, the most significant effect is from the presence of the dissolved material [23].

Microwave radiation is one section of the electromagnetic spectrum that takes advantage of this fact to measure salinity [23]. Microwave radiation does not require direct contact with the water to make a measurement, making it possible to measure the salinity of a water sample from a far distance, including from space [24]. This necessitated the investigation of the relationship that could accurately predict salinity from a microwave reading [24]. The relationship required multiple different corrections as the microwave readings were found to be affected by [Sea Surface Temperature \(SST\)](#), surface air pressure, surface air temperature, faraday rotation, and surface wind speed [14].

This research has allowed for the development of satellites that can measure the salinity, which has been used to develop global salinity maps as shown in Figure 2.1. The data measured using this method is reported to be accurate to within 0.1 on the Practical Salinity Scale PSS-78 [14].

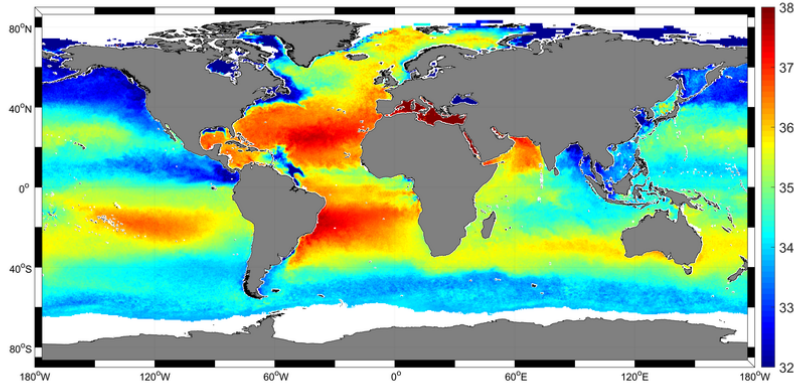


Figure 2.1: Global salinity map generated using satellite data [25].

2.4.5 Salinity from Refractive Index

The second measurement method that takes advantage of the electromagnetic spectrum interaction uses the visible light spectrum to measure the water's refractive index. The relationship between salinity and refractive index is similarly complex, requiring a 27-term equation that includes the effect of pressure and temperature. The refractive index equation is defined a range of 500 – 700nm in wave length, 0 – 30°C in temperature, 0 – 40 on the Practical Salinity Scale PSS-78, and 0 – 11000dbar in pressure, and it holds an accuracy of 0.4 – 80 [parts per million \(ppm\)](#) on the Practical Salinity Scale PSS-78, decreasing with increasing pressure. [26]

Refractometers are used to measures the refractive index of water and as only a small amount of the sample is needed, these devices are relatively compact. Two notably compact versions have dimensions of 22.5mm × 22.5mm × 120mm [15] and 40mm × 40mm × 70mm [27] which have achieved accuracies of 2 and 83 [%](#) on the Practical Salinity Scale PSS-78 respectively.

2.4.6 Salinity from Interferometry

The last measurement method that uses the electromagnetic spectrum is interferometry. Interferometry involves generating two identical light waves on the visible spectrum, passing one through the sample and the other through a non-interfering medium, and then comparing the two waves. The comparative gain and phase shift between the two waves can be used to identify the salinity of a sample of salt water [28].

This method has varying implementations, each with varying results. Reference [16] reported to be accurate within 0.001 on the Practical Salinity Scale PSS-78 using a Michelson interferometer and other researchers have reported other accuracies using different interferometers [29, 30, 31]. The refractometer has the disadvantage of being a large instrument requiring precisely aligned and spaced mirrors to direct the light waves, making it difficult to implement in a compact device.

2.4.7 Salinity from Magnetic Permeability

Similarly to conductivity, a liquid's magnetic permeability is related to the number of ions present in it. The more ions present in the liquid, the stronger the magnetic alignment that the liquid can generate, increasing its magnetic permeability. In salt water, this is related to the total dissolved solids [32].

Several methods are available for measuring a liquid's magnetic permeability, including [Inductance \(L\)](#), [Capacitance \(C\)](#), [Resistance \(R\) \(LCR\)](#) meters [33], resonant circuits [34], magnetic force sensors [35], and a permeability bridge [36]. These methods all have the advantage of not requiring direct contact with the salt water to make a measurement, which allows for the sample to remain undisturbed, unlike conductivity and other methods which may be destructive [37]. While the measurement of the magnetic permeability is well-defined, the relationship between it and salinity has yet to be thoroughly investigated. Additionally, the equipment required to measure the magnetic permeability is relatively large and typically has a high power consumption, making it difficult to compact for use in remote environments.

2.5 Salinity Measurement Devices using Conductivity

There are several commercial [CTD](#) devices available from small handheld devices such as the [Salinity Pen](#) to large oceanographic research devices such as [Ocean Exploration's CTD](#). These devices are used in various applications with varying prices and accuracies. The fundamental concept of the device involves placing two electrodes in a sample of water, applying a voltage across them, and measuring the water's response. This is paired with a temperature and depth correction, which allows a salinity value to be calculated, which is discussed in Section 3.1. Unfortunately, most of [CTD](#)'s technology is proprietary so the exact workings of their devices are not published.

Some researchers have developed their own [CTD](#) devices for specific applications. A study investigating the effect of human activities that alter the salt concentration of water sources such as lakes, ponds and wetlands in Illinois, USA, developed their own [CTD](#). The device reported an average error of 6% in the laboratory validation and 11% in the field validation. It used an alternative approximation of converting the conductivity to salinity, which used single voltage readings to measure the resistance of the water samples, which were then used to create a sensor-specific mathematical model to convert the resistance

2.5. Salinity Measurement Devices using Conductivity

to salinity [38]. A similar device was shown on a forum with a similar design principle; however, this one was significantly less advanced, making no attempt to correlate the measured resistance values to a salinity value [39].

Researchers at Uppsala University in Sweden developed a nano CTD probe that measured $7.5 \times 3.5\text{mm}$ in size, shown in Figure 2.2. The probe contained everything required for an accurate salinity measurement, and each of the sensors achieved a high degree of accuracy. The probe achieved a high r^2 value of 0.9787 and a standard deviation of 2.37% using an alternating current at 42kHz to measure the conductivity. This design indicated that miniaturized salinometers are viable and could be used in devices such as bio-loggers on marine animals. [40]

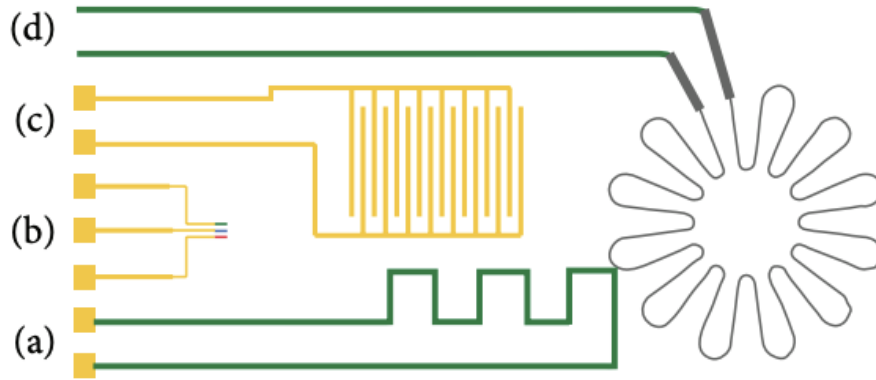


Figure 2.2: The schematic of a CTD probe developed by researchers at Uppsala University in Sweden which design contains (a) a temperature sensor, (b) three relatively small electrodes for pH and Cl-concentration, (c) conductivity electrodes, and (d) a strain gauge for the pressure membrane sensor.

The design is $7.5 \times 3.5\text{mm}$ in size [40].

Chapter 3

Theory Development

3.1 The Calculation of Salinity From Conductivity

Salinity meters that use electrical conductivity are commonly known as CTDs. As depth is a measurement derived from pressure, CT_p is the preferred designation when performing calculations [8], which allows for the conductivity of a sample of water to be denoted by $C(S, T, p)$ where conductivity is a function of salinity S , temperature T , and pressure p which is the convention in oceanography [8]. Pressure in the salinity equation is taken relative to sea level where $p = 0\text{dbar}$ is equivalent to an absolute pressure of $P = 101\ 325\text{Pa}$ [11]. Using decibars (dbar) for pressure is a common practice in oceanography as it is a unit of pressure roughly equivalent to one meter of water depth [41].

The Practical Salinity Scale defines Practical salinity S_p in terms of a conductivity ratio K_{15} , which is the conductivity of a sample of water at a temperature of 15°C and a pressure equal to one standard atmosphere divided by the conductivity of a standard potassium chloride solution at the same temperature and pressure. The standard potassium chloride solution is 32.4356g of KCl dissolved in 1.000kg of water, and when the ratio between the conductivity of a sample of water and the standard solution, or K_{15} , equals 1, the Practical Salinity S_p is, by definition, 35. [11]

When K_{15} is not equal to 1, the Practical Salinity S_p can be calculated using the PSS-78 equation shown in Equation 3.1.

$$S_p = \sum_{i=0}^5 a_i (K_{15})^{i/2} \quad \text{where} \quad K_{15} = \frac{C(S_p, 15^\circ\text{C}, 0)}{C(35, 15^\circ\text{C}, 0)} \quad (3.1)$$

All the coefficients for the salinity-conductivity equations, including a_i , are given in Table 3.1.

To calculate the salinity of a sample of water that is not at 15°C and 0dbar , the conductivity ratio of the sample can be expanded into the product of three ratios, which are labelled R_p , R_t , and r_t respectively. The conductivity measurement taken in the field $C(S_p, t, p)$ is related to the conductivity of the standard solution $C(35, 15^\circ\text{C}, 0)$ which the device is calibrated with and is represented by R in Equation 3.2. [11]

$$R = \frac{C(S_p, t, p)}{C(35, 15^\circ\text{C}, 0)} = \frac{C(S_p, t, p)}{C(S_p, t, 0)} \cdot \frac{C(S_p, t, 0)}{C(35, t, 0)} \cdot \frac{C(35, t, 0)}{C(35, 15^\circ\text{C}, 0)} = R_p R_t r_t \quad (3.2)$$

check In order to calculate the salinity of the sample, R_t must be found, which takes a similar form to

3.1. The Calculation of Salinity From Conductivity

K_{15} . r_t is first calculated using the temperature of the sample

$$r_t = \sum_{i=0}^4 c_i t^i \quad (3.3)$$

following which R_p is calculated using the sample's pressure p , temperature t and conductivity ratio R ,

$$R_p = 1 + \frac{\sum_{i=1}^3 e_i p^i}{1 + d_1 t + d_2 t^2 + R [d_3 + d_4 t]} \quad (3.4)$$

and finally R_t is calculated using r_t , R_p and R .

$$R_t = \frac{R}{R_p r_t} \quad (3.5)$$

For a sample temperature of $15^\circ C$ and pressure of 0dbar , r_t and R_t both equal 1, which leaves R_t equal to R and thus Equation 3.1 can be used to calculate the Practical Salinity S_p . For temperatures other than $15^\circ C$, the Practical Salinity S_p can be calculated using Equation 3.6 where $k = 0.0162$. [11]

$$S_p = \sum_{i=0}^5 a_i (R_t)^{i/2} + \frac{t - 15}{1 + k(t - 15)} \sum_{i=0}^5 b_i (R_t)^{i/2} \quad (3.6)$$

Table 3.1: Coefficients for the PSS-78 equations [11].

i	a_i	b_i	c_i	d_i	e_i
0	0.0080	0.0005	$6.766097 \cdot 10^{-1}$		
1	-0.1692	-0.0056	$2.00564 \cdot 10^{-2}$	$3.426 \cdot 10^{-2}$	$2.070 \cdot 10^{-5}$
2	25.3851	-0.0066	$1.104259 \cdot 10^{-4}$	$4.464 \cdot 10^{-4}$	$-6.370 \cdot 10^{-10}$
3	14.0941	-0.0375	$-6.9698 \cdot 10^{-7}$	$-4.215 \cdot 10^{-3}$	$3.989 \cdot 10^{-15}$
4	-7.0261	0.0636	$1.0031 \cdot 10^{-9}$	$-3.107 \cdot 10^{-3}$	
5	2.7081	-0.0144			

Note that the coefficients a_i precisely sum to 35 such that the Practical Salinity S_p is 35 when K_{15} or $R_t = 1$ as per Equation 3.1 and Equation 3.6. Additionally, the coefficients b_i precisely sum to 0 such that the Practical Salinity S_p does not depend on the temperature of the water when $R_t = 1$ as per Equation 3.6. [11]

Equation 3.1 to Equation 3.6 are valid for $2 < S_p < 42$ and $-2^\circ C < t < 35^\circ C$ and $0\text{dbar} < p < 10\,000\text{dbar}$ [11]. The range for salinity has been extended using estimations by Reference [42] for $0 < S_p < 2$ and Reference [43] for $42 < S_p < 50$.

The temperatures used in Equation 3.1 to Equation 3.6 are on the IPTS-68 scale [44] and have not been corrected to the currently used ITS-90 scale [45]. In order to correctly calculate the salinity, the

temperatures should be converted to the IPTS-68 scale using the equation $t_{68} = 1.00024t_{90}$ before calculating salinity [45].

3.2 Salt water's Resistance-Voltage Measurement

3.3 Current Fringing in Conductive Materials

Current fringing or current spreading, not to be confused with magnetic fringing, occurs when an electrical current flowing through a conductive material spreads like a magnetic field. This is a phenomenon that is particularly prevalent and well studied in the manufacturing of [Light Emitting Diodes \(LEDs\)](#) where the current spreading can be a significant factor in the efficiency of the device [46, 47, 48].

The effect of current spreading in typical conductors is mostly negligible; if the material's conductivity is high enough and its cross-sectional area is small, the current spreading is minimal. However, if a conductor has a significantly larger cross-sectional area than the current requires, such as electrodes in salt water, the current spreading can become a significant factor in its conductivity. This version of current spreading has been studied and is documented for conductors of constant conductivity. [49]

Chapter 4

Design

4.1 Salinity Measurement Method

The industry standard for measuring conductivity is the [CTD](#), which calculates salinity using conductivity, temperature and depth measurement. Section [2.4](#) discussed several alternative methods of measuring salinity. The temperatures, environment and remote nature of the Antarctic make most of these methods difficult or impossible to use. Additionally, the final device was required to fit through an ice core hole of 110mm in diameter. While the prototype does not need to directly meet this requirement, it must be designed such that a future iteration can.

Refractometers and chlorinity titrations have the same drawbacks as the currently used hand-held [CTD](#), where capturing a water sample and bringing it to the surface alters its temperature and pressure, which may alter its salinity measurement. Microwave radiation has a lower-than-desirable accuracy. In addition, the instruments that measure it, as well as densitometers and interferometers, are expensive and complex beyond the author's expertise. Electromagnetic induction is one of the more promising methods because it is a nondestructive method of measuring salinity, which allows samples to be used for alternative measurements afterwards. However, as mentioned in Section [2.4.7](#), the electromagnetic and salinity relationship has yet to be thoroughly researched, and it requires a high power consumption. This latter is a significant issue in Antarctica as storing power is challenging at very low temperatures, not to mention transporting the device.

The conductivity, temperature and depth method was determined to be the most viable for this project as it is the industry standard, and the author has significant experience with [Printed Circuit Board \(PCB\)](#) design and electronics. Additionally, it has been proven that it can be miniaturized, as mentioned in Section [2.5](#), making it the most likely method to fit through the ice core. This and the other methods face a challenge because the Practical Salinity Scale is not defined for sub-zero temperatures, which may be a problem in Antarctica and should be researched further.

4.2 Conductivity Electrode Material

Ideal electrodes for measuring conductivity in salt water have zero resistance and infinite corrosion resistance and can confine the electrical current in the water to a specific known volume. Electrodes with zero resistance would allow the resistance measured using the electrodes to be entirely due to the water. However, most conductive materials have a conductivity in the order of $10^8 Sm^{-1}$, which causes negligible resistance compared to salt water which has a conductivity range of $0 - 5Sm^{-1}$ [\[50\]](#).

The infinite corrosion resistance will allow the electrodes to last indefinitely in the highly corrosive saltwater environment, and several materials with near-perfect corrosion resistance are used in marine environments, which will be able to satisfy this criterion. The confinement of the electrical current allows for an easier calculation of the conductivity ρ from resistance R if the cross-sectional area A and length l of the water between the electrodes is known as shown by Equation 4.1.

$$\rho = \frac{RA}{l} \quad (4.1)$$

Several materials known for their corrosion resistance include non-precious metals such as aluminium, stainless steel, nickel and copper alloys, and titanium, as well as precious metals such as gold, silver, and platinum. Precious metals are known for having a significantly higher corrosion resistance. However, they are also significantly more expensive.

Choosing the electrode's material involved prioritising high corrosion resistance and low resistance while being restricted to materials that were attainable and within this project's budget. Titanium is the most corrosive resistant of the non-precious metals and has an acceptable conductivity of $2,3 \cdot 10^6$ which is about 25 less than that of copper [51]. Titanium wire was available through off-cuts from a project being conducted by the Chemical Engineering Department of the University of Cape Town. Thus, it was possible to use this material for the electrodes.

Of the precious metals, gold is one of the most accessible as it is a common material used in PCBs manufacturing primarily because of its high corrosion resistance paired with a high conductivity of $49 \cdot 10^6$ which is similar to copper's conductivity [51]. Electroless Nickel Immersion Gold (ENIG) PCB manufacturing is a process where nickel, followed by gold, is deposited onto the copper of the PCB using chemical reactions. While this process is expensive compared to standard PCB manufacturing, it is affordable within this project's budget and made gold a possible electrode material.

Both gold and titanium were used for this project, as they could be manufactured into electrodes of different shapes, which allowed for comparative testing of the materials and the shapes. The electrode design is further discussed in Section 4.3.

4.3 Conductivity Electrode Design

Gold electrodes made using the ENIG PCB manufacturing process were chosen as the device's primary electrodes. The PCB manufacturing process allowed the electrodes to be made with a known area and length of the water between the electrodes, allowing for a more accurate conductivity calculation.

Salt water does not have a constant resistivity with respect to voltage [38],[52]. In order to isolate the non-linear resistance-voltage curve, the resistance of the water between the electrodes needed to be measured at different voltages while other factors were kept constant. This necessitated close attention to the fringing effect of the electrical current between the electrodes. Wide, flat pads were used on the PCB electrodes, which were placed close together to reduce the current spreading. Additionally, a fringe guard was added to the electrodes, which consisted of a pad that outlined the main conductivity pads that repeated the same voltage as the main pads using an op-amp with unity gain. Ideally, the fringe guard would saturate the volume around the main pads with current and thus prevent them

from fringing. PCB connectors to attach the electrodes to a probe were added to this configuration, as shown in Figure 4.1.

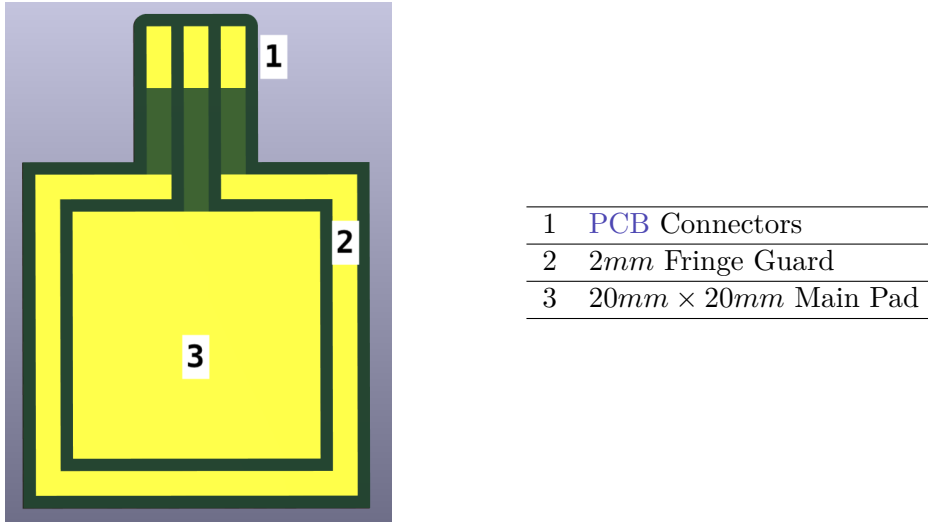


Figure 4.1: The gold electrode PCB design.

The dimensions of the gold electrodes were chosen to be round values, with the pads having a large surface area and being placed relatively close together. However, they could not be placed too close together as this could prevent water from effectively flowing between them. Theoretically, this would reduce the proportion of fringing versus linear current between the electrodes. This theory is based on the electrical field fringing effect found in capacitors: take two capacitor pads that are placed close together, which experience a certain amount of fringing; if the area of those two pads increases, the quantity of fringing field will increase relative to the side length while the quantity of linear field which would increase relative to the square of the side length [53, 54].

The second method employed to reduce the fringing effect was to keep the resistance between the pads low, which lowers the voltage required to generate a current through the water, which would theoretically further reduce the current fringing. This theory is also based on capacitors where higher voltages generate stronger electrical fields that spread, or fringe, more.

The gold electrodes were designed with a $20\text{mm} \times 20\text{mm}$ main pad with a 2mm wide fringe guard surrounding it and a spacing between the electrodes of 10mm . The expected resistance was then calculated to be between $3,75\Omega$ and $6,25\Omega$ using Equation 4.1 and conductivity values for salinities between 40 and 25 on the Practical Salinity Scale PSS-78 [11].

The titanium electrodes were less complicated to design as they only had two variable parameters: their length and spacing. However, as they were made from titanium wire, the fringing effect between them could not be reduced using the same method as the gold electrodes. Thus, it was decided to use the gold electrode to evaluate an accurate method for determining conductivity, which could then be applied to the titanium electrodes, where the fringing effect could be mathematically corrected.

The titanium electrodes are significantly more cost-effective than the gold electrodes. Thus, if an accurate method for determining salinity using them is developed, they will likely become the primary electrodes of the final device. The titanium wire available for this project was 1mm in diameter and to

account for the unknown resistance between the electrodes, the design allowed for adjustable spacing between the electrodes and adjustable electrode length.

4.4 Resistance Measurement Method

The most common and practical method of measuring resistance is using a resistor divider circuit, which this project chose to employ. While current measuring [Integrated Circuits \(ICs\)](#) exist, the low current ($< 1A$) versions use the same resistor divider principle. Thus, it was considered to be more cost-effective and configurable to design the resistor divider circuit.

The electrodes were chosen to be the R_2 resistor in the voltage divider, and the R_1 resistor was chosen to be a significantly larger, known resistance. The large R_1 value allowed a full range of voltages to be applied to the resistor divider while keeping the voltage across the electrodes low, which was advantageous for the reasons mentioned in Section 4.3. This configuration also prevented the circuit from being short-circuited if the electrodes were to touch, as the R_1 resistor would limit the current. The voltage drop across the electrodes was then amplified using an op-amp to increase the resolution of the voltage measurement.

4.5 Circuit Overview

The resistor divider circuit was designed to be printed onto a [PCB](#) (herewith referred to as the probe) manufactured with JLCPCB. [PCB](#) manufacturing is cost-effective, has a high precision relative to hand soldering, and the process was familiar to the author, making it the ideal method for creating the prototype. However, the resistor divider circuit required a few additions to increase its versatility and testing capability, an overview of which is shown in Figure 4.2.

The voltage driving the resistor divider was provided by a [Digital to Analogue Converter \(DAC\)](#) so that the voltage could be varied and salt water's voltage-resistance relationship could be determined. The [DAC](#) model was chosen from the [DACs](#) available on the JLCPCB's website. The model DAC53401 was ultimately chosen for its high updated time of $10\mu s$ and its advanced functionality, which allowed it to output square, triangle, and sawtooth waves. This functionality could be used to perform high-frequency tests in addition to linear voltage sweeps.

A typical configuration of a [DAC](#) is to connect its output to the non-inverting input of an op-amp, which would be connected to the base of a transistor. The transistor's emitter would then be connected to the inverting input of the op-amp. This configuration allows a higher current to be drawn than the [DAC](#) can provide while maintaining the specified output voltage. The DAC53401 has an internal op-amp and a feedback input, which allows a transistor to be connected as shown in Figure 4.2 to achieve the same outcome.

Sets of switches added to the circuit allowed the voltage produced by the [DAC](#) to be directed to an R_1 resistor, then across to a pair of electrodes or to a calibration resistor. The switch model TS3A4751 was chosen from JLCPCB, which contained four switches in its [IC](#), as it was very cost-effective for its low and consistent on-state resistance of around 0.7Ω . The circuit required three switching points: one for choosing the R_1 resistor, one for choosing the anode and one for choosing the cathode.

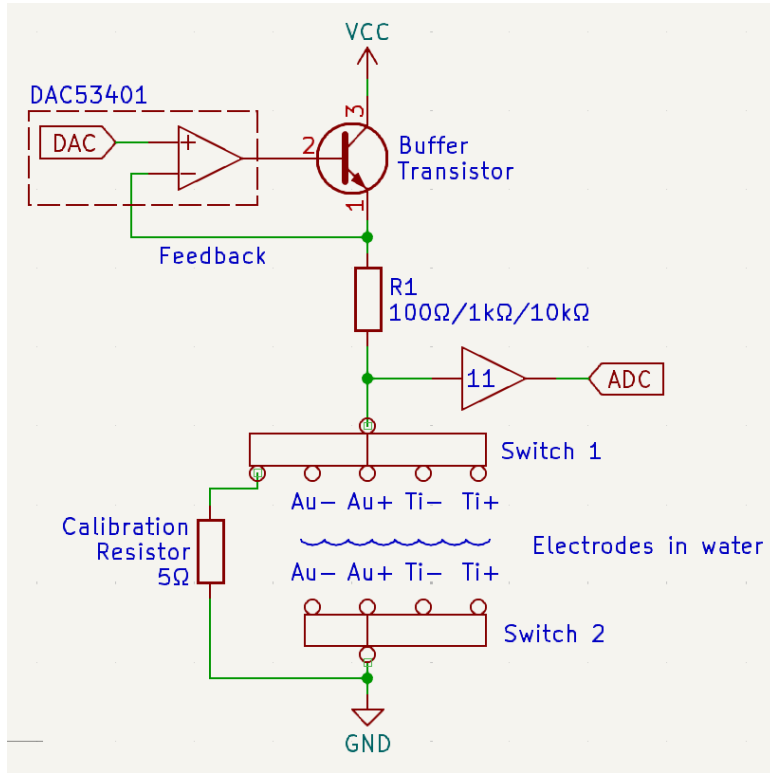


Figure 4.2: A simplified representation of the resistance measuring circuit.

It was decided to give the R_1 resistor alternate resistances to allow for any possible resistance between the titanium electrodes or unforeseen errors. The R_1 value chosen to pair with the gold electrodes was 100Ω as it was the smallest e12 series resistance that would prevent the board from drawing too much current and burning out the traces or switches. The final resistances were chosen to be 100Ω , $1k\Omega$ and $10k\Omega$, which would be used when the resistance between the probes was $1\Omega - 10\Omega$, $10\Omega - 100\Omega$ and $100\Omega - 1k\Omega$ respectively. This configuration allowed for a minimum resolution of 11% of V_{DAC} for the voltage measurement by the [Analogue to Digital Converter \(ADC\)](#) as shown by Equation 4.2.

$$\frac{1\Omega}{1\Omega + 100\Omega} * V_{DAC} * 11 = 11\%V_{DAC} \quad (4.2)$$

$$\frac{10\Omega}{10\Omega + 100\Omega} * V_{DAC} * 11 = 100\%V_{DAC} \quad (4.3)$$

The anode switch, denoted as switch 1 in Figure 4.2, allowed R_1 to be connected to any of the four electrodes or to the calibration resistor of 5Ω , and the cathode switch, denoted as switch 2 in Figure 4.2, allowed any electrode to be connected to ground. An example of measuring the resistance between the titanium electrodes would be to connect switch 1 to Ti^+ and switch 2 to Ti , allowing the voltage drop to be measured. This configuration also allows current to flow in both directions between electrodes, which can prevent an excessive buildup of chlorine gas or sodium electroplating on the electrodes or electrolysis of the water by taking a resistance measurement in both directions in rapid succession.

To increase the accuracy of the R_1 resistors, they were made by placing multiple high-accuracy resistors in parallel, which decreases their resistance uncertainty. The total uncertainty of the parallel resistance $\delta_{R_{total}}$ is decreased by a factor equal to number of parallel resistors n compared to each resistance's

uncertainty δ_R as shown by Equation 4.4 to Equation 4.6.

$$R_{total} = \left[\sum_{i=1}^n \frac{1}{R_i} \right]^{-1} = \left(\frac{n}{R} \right)^{-1} = \frac{1}{n} \cdot R \quad (4.4)$$

for a function $f(x_1, x_2, \dots, x_n)$, its tolerance $\delta_f = \sqrt{\sum_{i=1}^n \left(\frac{\partial f}{\partial x_i} \delta x_i \right)^2}$ (4.5)

$$\therefore \delta_{R_{total}} = \sqrt{\left(\frac{\partial R_{total}}{\partial R} \delta R \right)^2} = \sqrt{\left(\frac{1}{n} \delta R \right)^2} = \frac{1}{n} \delta_R \quad (4.6)$$

The R_1 resistors were made from 3 parallel resistors, each with tolerance $\pm 1\%$ giving a total tolerance of $\pm 0.3\%$ and the calibration resistor was made from 4 parallel resistors with tolerance $\pm 1\%$ giving a total tolerance of $\pm 0.25\%$.

A last switch point was added to the circuit for the gold electrode's fringe guards, an example of which is shown in Figure 4.3. The voltage from R_1 was routed to a buffer op-amp with unity gain. Its output was then connected to the fringe guard, which effectively repeated the same voltage as the main pad while not affecting any measurements using them. The other fringe guard could be switched to ground, allowing a current to be generated between the two. This current would ideally absorb any possible fringing from the main pads. The same switch point also allowed the fringe guards to be electrically disconnected to test their effectiveness and to determine if they interfered with the measurement. Lastly, as the fringe guards held the same voltage difference as the main pads and, in theory, had a higher resistance due to their smaller area, the current flowing between them was assumed to be less than that of the main pads; thus, there was no need to limit the current from the op-amp.

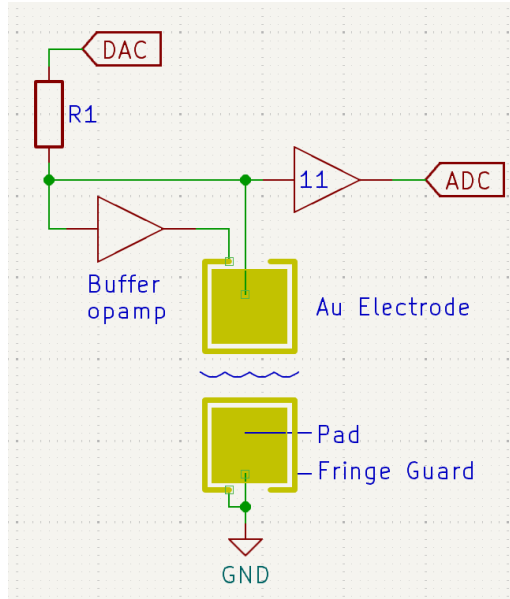


Figure 4.3: A simplified representation of the resistance measurement circuit using the gold electrodes with the fringe guard.

4.6 Salinity Calculation and Display

In order to measure the salinity of the water, the probe [PCB](#) would be lowered through the ice core hole into the water to capture salinity readings at various depths. The measurements could either be captured automatically at preprogrammed depth or time intervals or triggered by the user using a controller. The latter method was chosen for this project because it is a more user-friendly approach, allowing researchers to control precisely which depths the salinity measurements are made and giving them live updates about the probe's status and onboard sensors.

The controller was a straightforward [PCB](#) with input buttons and rotary switches, two 7-segment displays, a [Recommended Standard #485 \(RS-485\)](#) communication port and a simple microcontroller.

Saltwater has a high [Electromagnetic Interference \(EMI\)](#), which interferes with all wireless communication [55]. While high-power wireless communication is viable for ranges up to 70m, it is more reliable, cost-effective, and power efficient to use a wired connection [56]. [RS-485](#) is a robust, long-range embedded communication protocol that only requires a simple [IC](#) to use, making it ideal for this project. Additionally, the author was familiar with this protocol and had previous board-to-board communication experience with it.

[Universal Asynchronous Receiver-Transmitter \(UART\)](#) to [RS-485](#) converters are common as most microcontrollers have a [UART](#) communication port. This project used half-duplex [RS-485](#) as it is the industry standard, and it is more cost-effective than full-duplex [RS-485](#), which requires an additional [UART](#) to [RS-485](#).

The microcontroller was chosen from the STM32F030 series as it did not need to perform any complex calculations, and the author was familiar with this series.

With an external controller, a waterproofed probe could be lowered into the water to measure its salinity. The chosen method of waterproofing the probe was to coat it with epoxy resin, as this was the most familiar and cost-efficient method available. The other notable option is to create a waterproof housing for the probe, but this can be complex and expensive. In addition to the circuitry shown in Figure 4.2, the probe had a temperature and depth sensor, which are discussed in Section 4.7, an [RS-485](#) communication port and a microcontroller. The microcontroller was chosen from the STM32F4 series as it is the most cost-effective series with a [Floating Point Unit \(FPU\)](#), allowing the salinity to be calculated on board as per the equations in Section 3.1.

4.7 Temperature and Depth Measurement

Waterproof depth sensors were too expensive for this project's budget, costing around \$100. An alternative approach is to use a non-waterproof pressure sensor that is isolated from the water using a flexible membrane that allows the external pressure to be transmitted to the sensor. The WF183DE pressure sensor was chosen as it was the most cost-effective sensor rated for above 50 meters of water pressure available at [JLCPCB](#). Should this approach fail, the backup plan was to use the controller to manually input a depth so that the salinity could still be calculated.

The temperature sensor was an arbitrarily chosen surface-mount sensor with high accuracy of $\pm 0.3^{\circ}\text{C}$

4.7. Temperature and Depth Measurement

and a wide temperature range of -45 to 130°C . Epoxy resin is a poor thermal conductor [57]. Thus, the temperature sensor should be coated with a very thin layer of epoxy when the probe PCB is cast, allowing for a more accurate measurement. The choice of microcontroller and pressure sensor also provided this board with two alternative temperature sensors, which were less accurate but could be used in the event that the primary temperature sensor failed.

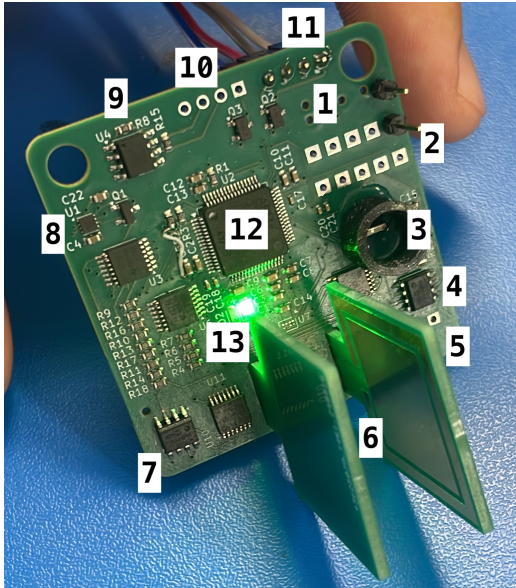
Chapter 5

PCB Construction, Adjustments and Code

5.1 PCB Design

The probe, controller and gold electrodes were fabricated on [PCBs](#), which were designed using KiCad software and manufactured with JLCPCB. The KiCad design files can be found in the Git repository linked in Appendix ???. The gold electrodes were trivial, only requiring a single layer [PCB](#) with simple pads and traces.

The probe [PCB](#) was the most complex. It was fabricated on a 4-layer [PCB](#) with dimensions of $50 \times 50\text{mm}$, shown in Figure 5.1. JLCPCB offered a discount for 4-layer [PCBs](#) that were smaller than $50 \times 50\text{mm}$ in size. While the probe should ideally be as small as possible to fit through the ice core, it was not designed to be smaller than $50 \times 50\text{mm}$ to allow for a more straightforward debugging process.



1	Programmer Port
2	Test Points
3	Pressure Sensor in a Protective Housing
4	11x Gain Op-Amp
5	Titanium Electrode Port
6	Gold Electrodes
7	Unity Gain Buffer Op-amp
8	DAC and Buffer Transistor
9	UART to RS-485 Converter
10	RS-485 Port
11	UART Port
12	STM32F4 Microcontroller
13	LEDs

Figure 5.1: The probe PCB with the gold electrodes attached and some adjustments made

Note 1: The rest of the titanium electrode ports are behind the gold electrode.

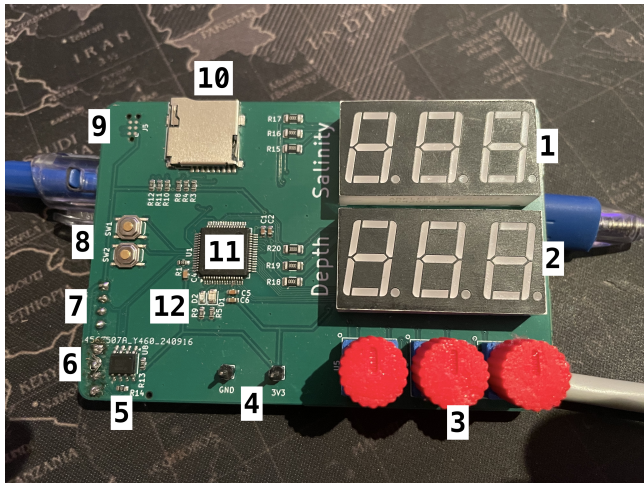
Note 2: The other ICs present are the TS3A4751 switches.

The probe was designed with the resistance measuring circuitry, the temperature and pressure sensors, the microcontroller, the [UART to RS-485](#) converter and the [RS-485](#) port mentioned in Chapter 4.

The gold and titanium electrode ports, which were placed at the bottom of the probe, were designed to allow them to be soldered perpendicular to it. The other methods of attachment all presented a fundamental disadvantage: connecting them with wires added extra resistance, and attaching them parallel to the board or perpendicular facing downwards was considered too complex.

Several adjustments were made to facilitate easier debugging. A [UART](#) port was added next to the [RS-485](#) port to allow for data to be streamed to a computer using a [UART](#) to [Universal Serial Bus \(USB\)](#) converter. Both ports also had reverse polarity protection added to prevent unintentional board damage. [LEDs](#) were added next to the microcontroller, and a programmer port and test points were added at the top of the board to allow for visual feedback and circuit analysis. With the programmer and communication ports at the top of the board and the electrodes at the bottom, the probe could safely be submerged while transferring its data to a laptop.

The controller [PCB](#) was fabricated on a 2-layer board, which is shown in Figure 5.2, as the components were too large to fit on a $50 \times 50\text{mm}$ 4-layer board. JLCPCB offered a similar discount for 2-layer [PCBs](#) that were less than $100 \times 100\text{mm}$ in area. Ultimately, the controller dimensions were $100 \times 60\text{mm}$, which could comfortably fit all the components while taking advantage of JLCPCB's discount.



1	Salinity 7-Segment Display
2	Depth 7-Segment Display
3	Rotary Switches
4	Power Input
5	UART to RS-485 Converter
6	RS-485 Port
7	UART Port
8	Input Buttons
9	Programmer Port
10	SD Card Port
11	STM32F0 Microcontroller
12	LEDs

Figure 5.2: The controller PCB with the rotary switch caps attached

The controller was designed with the buttons, the rotary switches, the 7-segment displays, the [UART](#) to [RS-485](#) converter, and the [RS-485](#) port mentioned in Chapter 4. The 7-segment displays were designated to display the salinity and depth of the water by default using silkscreen text, but they could be changed to display anything using software. The components were placed user-friendly, allowing for easy use of the buttons and rotary switches. Similarly to the probe, [LEDs](#), a [UART](#) port and a programmer port were added to the board to allow for debugging of the board. It should be noted that an SD Card Port was added for future development and testing but was not utilised during this project.

5.2 PCB Adjustments

Three adjustments were made to the probe [PCB](#) to ensure it functioned as required, excluding the soldering of headers and the gold electrodes. Firstly, one of the microcontroller's pins was unconnected

to power and was corrected by soldering a wire between it and a pin with power, which can be seen on the left of the microcontroller. Secondly, the footprint of the pressure sensor was horizontally reversed, which was corrected by flipping and soldering the depth sensor vertically. A protective case was added around the pressure sensor to prevent it from being damaged during testing. The casing would later function as the support for the waterproof membrane mentioned in Section 4.7.

Lastly, both op-amps were incorrectly chosen as they required a rail-to-rail voltage of 6V to operate, higher than the 3.3V provided. Thus, they were replaced with an alternative op-amp model with the same footprint. The temperature sensor also had an incorrect footprint, but this could not be rectified as it was discovered after the board was fabricated. Thus, the temperature sensor was not soldered to the board. The pressure sensor's onboard temperature sensor was used instead.

The controller PCB required no soldering adjustments. There was a minor error in the pin assignments of the rotary switches, but this was corrected in the software and did not require any hardware changes. Switch caps were 3D printed and attached to rotary switch shafts to make them easier to turn, making the controller more user-friendly.

5.3 Probe Code

The significant steps in measuring salinity are measuring the water's conductivity, temperature and pressure and then calculating its salinity. An overview of this process is shown in Figure 5.3.

The conductivity measurement was aimed at repeating the methodology that Reference [38] employed. This requires a voltage sweep of the water sample, which is then mapped to a conductivity. This devices specific mapping will have to be determined experimentally, as it is unique for different electrode sizes and materials. The voltage sweep is achieved by incrementing the output of the DAC from a given start to end voltage. At each step, the output of the DAC and the voltage drop across the calibration resistor and the electrodes are recorded.

To determine the resistance measuring accuracy, the resistance across the electrodes R_E was calculated using the voltage drop across the electrodes and across the calibration resistor R_C , as shown in Equation 5.1 to Equation 5.3. The electrode resistances R_E was calculated for each voltage sample and then averaged.

$$V_{ratio} = \frac{V_{DAC}A_{11}A_{ADC}\frac{R_E}{R_1 + R_E}}{V_{DAC}A_{11}A_{ADC}\frac{R_C}{R_1 + R_C}} = \frac{\frac{R_E}{R_1 + R_E}}{\frac{R_C}{R_1 + R_C}} \quad (5.1)$$

$$\frac{R_E}{R_1 + R_E} = V_{ratio} \frac{R_C}{R_1 + R_C} \rightarrow k \quad (5.2)$$

$$R_E = \frac{kR_1}{1 - k} \quad (5.3)$$

This method of calculating resistance using a voltage ratio with a known resistance allows the probe to nullify all scalar inaccuracies in the circuit, including the DAC, ADC and op-amp gain error, as

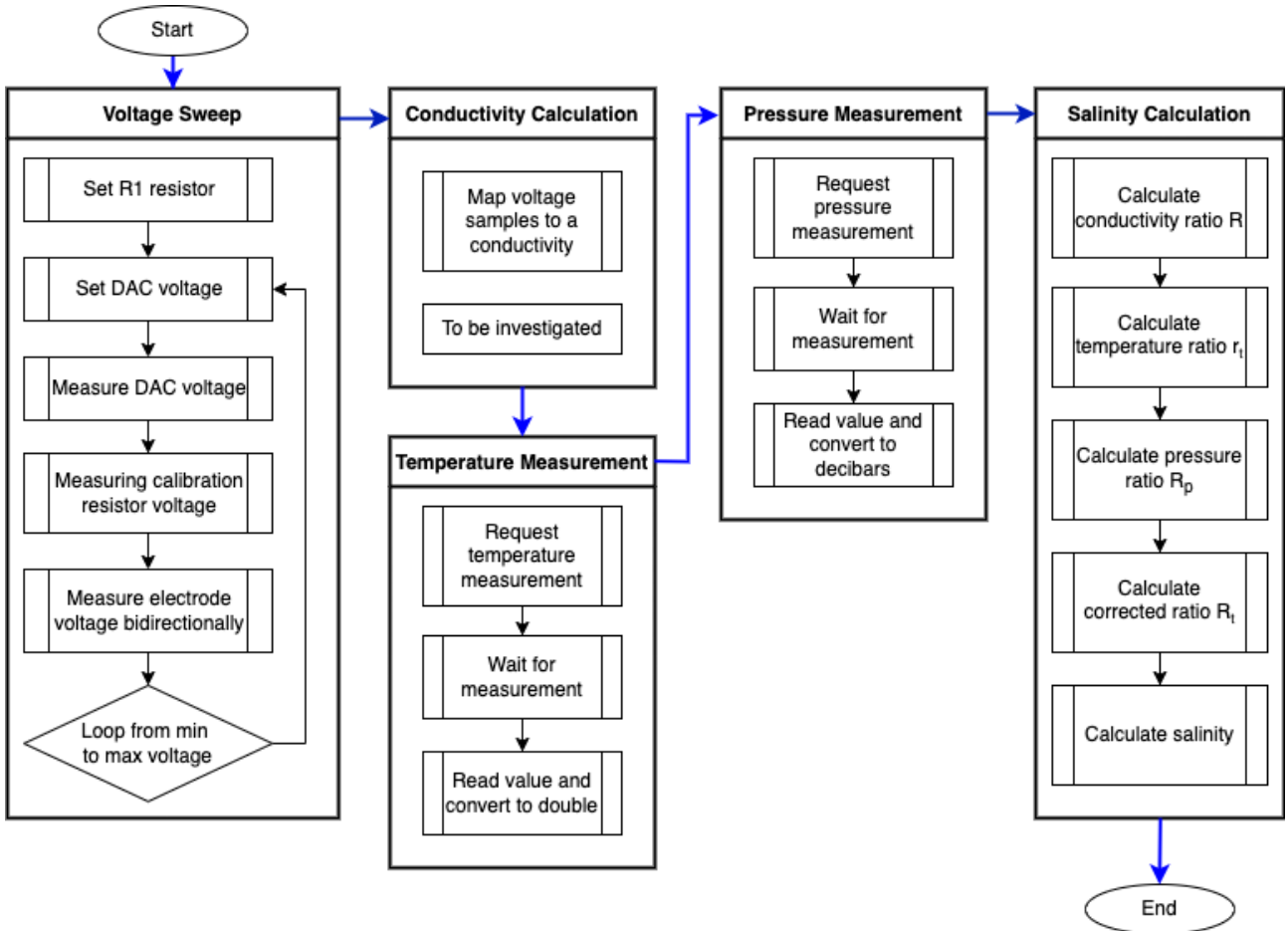


Figure 5.3: The flowchart for the probe code that measures salinity.

they will be present in both voltage measurements. However, this method is still vulnerable to offset inaccuracies, including **DAC** and **ADC** offset errors, op-amp input offset and input bias currents, the R_1 resistance errors and the resistance added by the switches and traces.

As previously mentioned, the pressure and temperature measurements are taken from the WF183DE pressure sensor. This sensor operates similarly for both measurements: a request is made to make a measurement, it can then be polled until the measurement is ready, and then the measurement can be read.

Once the conductivity, temperature and pressure measurements are taken and converted into the required units of Sm^{-1} , $^{\circ}C$ and $dbar$ respectively, salinity can be calculated as shown in Section 3.1. Additionally, if requested, any of the temperature, depth, resistance, or conductivity measurements can be calculated individually and transmitted to the controller.

5.4 Controller Code

The controller's primary function for the prospective user was to instruct the probe to take a measurement and display it. However, the controller was given additional functionality for testing and investigation purposes, which allowed the controller to update the probe's configuration.

The common-cathode 7-segment displays displayed the various measurements from the probe. The displays' digits were individually written to by writing the digit code and keeping the corresponding

digit's cathode low while keeping the others high. A timer controlled [Direct Memory Access \(DMA\)](#) was used to write to each digit in quick succession, giving the illusion of all the digits being on simultaneously.

The leftmost rotary switch was used to navigate the menu, which consisted of the default showing both salinity and depth, individual measurements of temperature, depth, resistance, conductivity, and salinity, and the probe's configurable parameters. The menu names were displayed on the top 7-segment display, and the selected menu item was displayed on the other. This created some limitations on what could be displayed. For instance, the best display of the word 'temperature' was 'teP', but all menu items had a unique, relatively clear name.

When the user selected a measurement menu item, the top switch was configured to request that measurement from the probe and display it; when the user selected a configuration menu item, the top switch was configured to update the probe's configuration. The other two rotary switches adjusted the probe's configurable parameters, further discussed in Section 5.5. The bottom switch was configured to reset the probe and the controller should an error occur.

5.5 Board-to-Board Communication

The probe and controller communicate using half-duplex [RS-485](#), which is converted on both sides to [UART](#). This makes the protocol effectively half-duplex [UART](#) communication from the perspective of the microcontrollers. The probe was configured to be in receive mode, where it would perpetually wait for a one-byte command from the controller. All the possible commands and expected transactions are shown in Figure 5.4.

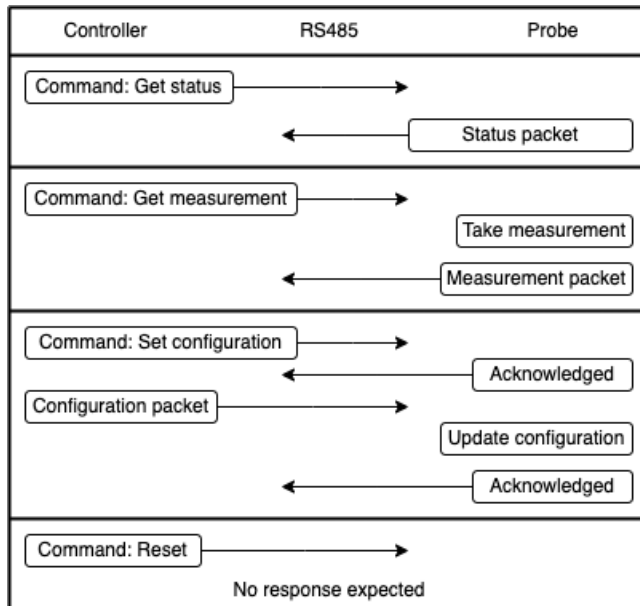


Figure 5.4: The flowchart for the board-to-board communication protocol denoting the four transaction types. The arrows denote the direction of the packets being sent over the [RS-485](#) link.

While not directly available to the user, the controller could request a status byte to which the probe would respond with *idle*, *busy* or *error* depending on its state. This allowed for some simple error

checking and communication flow, which could be integrated into more robust error handling in the future. When the user requests a measurement, the controller sends the corresponding request command, to which the probe will respond with the measurement data. The data was returned as a 3-byte, fixed-point float.

When the user requested a configuration update, the controller transferred a configuration packet using the expected transaction. Once the probe was entirely cast in epoxy resin, the configuration could only be updated this way, so all possibly useful, configurable parameters are included. This included which electrode to use (including whether to use the fringe shield), the R_1 resistor to use, the directionality of the resistance measurement (unidirectional or bidirectional), the voltage sweep start, end and number of steps, among other parameters. Some parameters, such as the directionality, were unlikely to be changed from their default value (bidirectional) but were included to cover any unforeseen circumstances.

When the user resets the boards using the controller's bottom switch, a reset command was sent to the probe before the controller reset itself. This command allows for resetting the probe should a system error occur. However, this only works provided the [RS-485](#) link is still operational. Otherwise, the entire system must be powered off and on again to reset the probe. The reset on both microcontrollers is triggered using software to set the [System Reset Request \(SYSRESETREQ\)](#) bit in the [System Control Block \(SCB\)](#) register, which triggers a system reset similar to pulling the reset pin low.

5.6 Probe Epoxy Casting

The circuitry on the probe had to be protected from the salt water while the electrodes were submerged, which was achieved using *Kristal 20* epoxy resin. Before casting the epoxy, the [RS-485](#) ports on the controller and probe were connected using a multicore cable, which connected their power, ground and the [RS-485](#) data lines, which can be seen in Figure 5.5. A casting mould was created using acrylic sheets, which are commonly used for epoxy moulds as they tend not to stick to the epoxy. The sheets were cut and secured using hot glue, as seen in Figure 5.6.



Figure 5.5: A top view of the probe casting mould, the controller and the connecting cable.

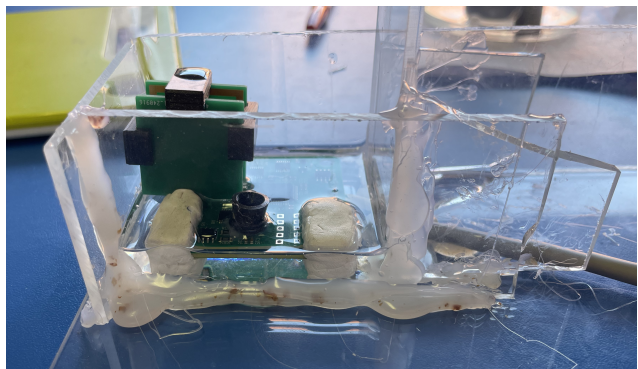


Figure 5.6: A side view of the probe casting mould showing the gold electrode spacers.

The gold electrodes were precisely spaced using 3D-printed spacers, which were attached during the casting process and removed once the epoxy had cured. Lastly, two areas of the probe still needed to be accessed: the programmer and [UART](#) ports and the titanium electrode ports. This would simplify

further testing and allow the titanium electrodes to be optimally spaced through experimentation instead of estimations. These areas were isolated using *Prestick*, a rubber-based reusable putty adhesive. The adhesive was removed after the epoxy had cured, allowing access to the aforementioned areas.

The probe was removed from the mould after the epoxy had cured, shown in Figure 5.7. The *Prestick* adhesive was relatively easy to remove, and the desired areas were still accessible, allowing the titanium electrode to be added. Titanium is challenging to solder, requiring a complex process and advanced machinery that was not available for this project [58]. Instead, thin copper wire was tightly wrapped around the last 5mm of the titanium electrode, which was folded over to secure the copper wire, as shown in Figure 5.8. This configuration made connecting the electrodes to their ports easy using standard soldering and provided a continuous connection between the probe and the titanium electrode.

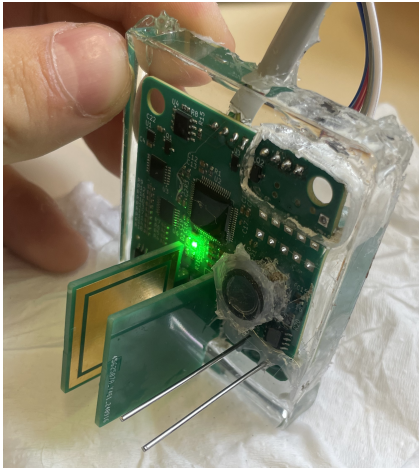


Figure 5.7: The probe after the epoxy casting process with the titanium electrodes and pressure sensor's flexible membrane attached.

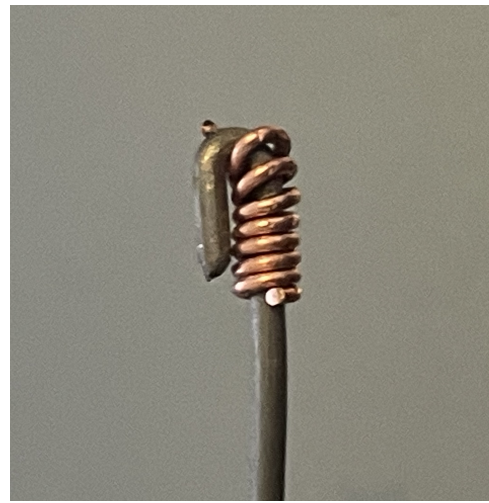


Figure 5.8: A close-up of the titanium electrode with the copper wire attached.

The unevenness of the mould and the hot glue created some rough edges along the epoxy. These could be laser cut to a smooth finish for the final product, but this was considered unnecessary for the experiments conducted in this project.

Lastly, hot glue was used to attach a flexible membrane to the pressure sensor's protective casing. The membrane was taken from the packaging of the gold electrode PCBs as it was readily accessible and had the required flexibility and durability to prove the concept. The final device would require further investigation into a more suitable material. The protective casing was also coated in a thin layer of hot glue as the 3D printing process used to create it had a small probability of being porous.

Chapter 6

Salinometer Evaluation and Testing

6.1 Overview

Several tests were conducted to evaluate the salinometer. The tests experimentally verified the accuracy of the individual components, evaluated the salinometer's interaction with saltwater samples and determined its ability and accuracy in measuring salinity. The tests were conducted in two phases because some required access to the board's circuitry and test points, while others required the probe to be exposed to salt water, which could only happen after the probe was cast in epoxy. The first phase involved evaluating the [DAC](#), [ADC](#), calibration resistor and resistance measuring accuracy which is covered in Section [6.3](#) to Section [6.6](#).

After the first testing phase, the probe was cast into epoxy resin as described in Section [5.6](#), which allowed the second phase to commence. The second phase involved establishing a voltage-resistance relationship for the salt water, a voltage-to-conductivity relationship for both electrodes and finally, the salinometer's ability to measure salinity, which is covered in Section ?? to Section ?. A summary of these tests is shown in Table [6.1](#), and each test is discussed in further detail in their relevant sections.

Table 6.1: A summary of the evaluation and testing of the salinometer.

Sec.	Test Description	Result Metric	Ideal Result	Measured Results
6.3	The minimum and maximum voltage output of the DAC between $0V$ and $V_{DD} = 3,3V$	Range	$0 - 3,3V$	$0 - 2,59V$
6.3	The gain and offset of the output voltage of the DAC relative to the instructed voltage	Gain	1,0	0,9837
		Offset	$0,0V$	0,0070V
6.4	The gain and offset of the voltage measured by the ADC relative to the voltage measured by the multimeter	Gain	1,0	0,9877
		Offset	$0,0V$	0,0082V
6.5	The resistance of the calibration resistor R_{CAL}	Resistance	5Ω	$5,00\Omega$
6.6	The gain and offset of the resistance measured by the salinometer relative to the resistance measured by the multimeter	Gain	1	1,0000
		Offset	0Ω	0,0000 Ω

6.2 Testing Apparatus

Voltage and resistance measurements were taken on the probe using a bench multimeter. The most accurate multimeter available was a *Keysight Technologies* U3401A, shown in Figure 6.2, which had voltage accuracy of 0,02% and resistance accuracy of 0,1%. In order to test the probe [PCB](#), voltage probes were connected to the test points, shown in Figure 6.1, or they were connected directly to the components.

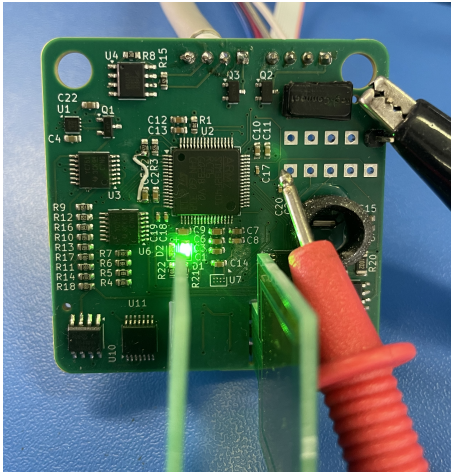


Figure 6.1: The salinometer probe with multimeter cables attached to a test point and ground.



Figure 6.2: The bench multimeter used for the tests displaying a voltage reading.

6.3 DAC Voltage Range and Accuracy

The transistor buffer configuration explained in Section 6.3 has one disadvantage: the output voltage of the system is limited by the transistor's V_{BE} where the highest possible voltage output is $V_{DD} - V_{BE}$. According to the transistor's [data sheet](#), the buffered output should be limited to $3,3V - 0,6V = 2,7V$ when conducting $0A$ and $3,3V - 0,75V = 2,55V$ when conducting the circuit's maximum current of $33mA$. In order to assess the range and accuracy of the [DAC](#), it was instructed to output voltages from $0V$ to $V_{DD} = 3,3V$ in intervals of 64-bit. The output voltage was measured at the base and emitter of the transistor, with no load and a maximum load of 100Ω . The results were graphed and shown in Figure 6.3 and Figure 6.4.

The voltage drop due to V_{BE} can clearly be seen on Figure 6.4. The unloaded output voltage reached $2,83V$, and the loaded output voltage reached $2,59V$, which were slightly higher than the predicted limits.

An alternative attempt was made to achieve a higher voltage output using the [DAC](#)'s internal voltage reference of $1,21V$ multiplied by a gain of 4, resulting in a reference of $4,84V$. As expected, this did not increase the output voltage; the base of the transistor continued to measure $3,3V$ and the emitter $2,83V$ while unloaded.

Due to the voltage limitations, the [DAC](#) was limited to $2,6V$ for future testing and implementation. When excluding the voltage readings above $2,6V$, the [DAC](#) achieved a gain of $0,9837V/V$ and an offset

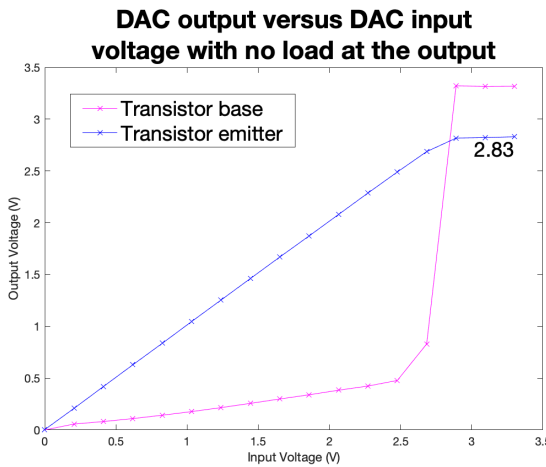


Figure 6.3: The input voltage versus the output voltage of the **DAC** with no load.

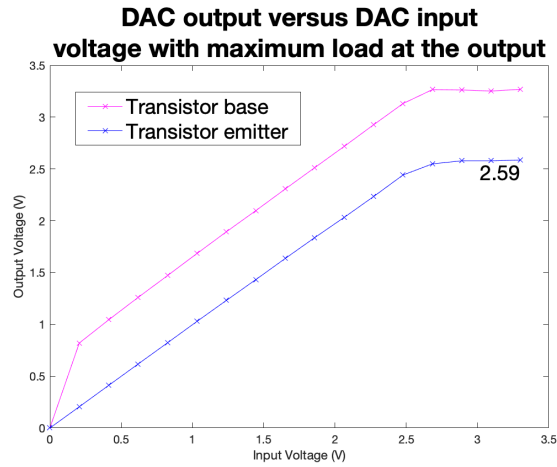


Figure 6.4: The input voltage versus the output voltage of the **DAC** with the maximum load of 100Ω .

+0,0070V between the input voltage and measured voltage under maximum load.

6.4 ADC Accuracy

The **ADC** was tested by measuring a range of voltages produced by the **DAC** and comparing them to the multimeter's measurement. The **ADC** was configured in 12-bit mode, with each measurement taking 15 **ADC** clock cycles, equivalent to 250ns with the 16MHz system clock. 5 measurements were taken and averaged for each voltage outputted by the **DAC** to increase the accuracy of each measurement. The results were graphed and shown in Figure 6.5.

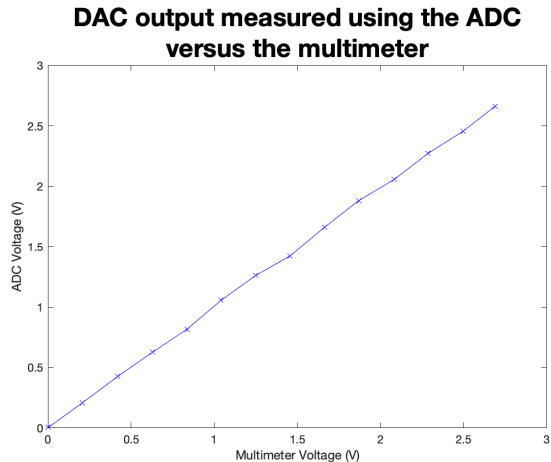


Figure 6.5: The voltage output by the **DAC** measured by a multimeter versus by the **ADC**.

The **ADC** achieved a gain of $0,9877\text{V/V}$ and an offset of $0,0082\text{V}$ compared to the multimeter.

6.5 Calibration Resistance

The multimeter measured the calibration resistor by directly connecting its probes to the four parallel resistors. The calibration resistor was electrically disconnected from the rest of the circuit during the measurement. The calibration resistance was specified to be $5\Omega \pm 0,25\%$; thus, its actual value could range between $4,9875$ and $5,0125\Omega$.

The multimeter measured the calibration resistor to be $5,25\Omega$. However, the multimeter probes measured $0,25\Omega$ when short-circuited. Thus, the actual resistance was calculated as $5,00\Omega$. It should be noted that the multimeter can only display to the nearest $0,01\Omega$. Thus, the actual resistance could range from $4,995\Omega$ to $5,005\Omega$, and more precise equipment would be required to obtain a more accurate measurement.

6.6 Resistance Measuring Accuracy

The probe's accuracy in measuring resistance was determined by comparing its calculated resistance to the multimeter's measurement of a given resistor. The probe calculated resistance by measuring the voltage drop across the resistor attached between the titanium electrode ports and the calibration resistor. Then, it calculated its resistance per Equation 4.4 to Equation 4.6.

For this test, the probe measured resistance using two methods: one with a single voltage provided by the DAC of $V_{DD}/2 = 1,65V$ and one with voltage sweep from the DAC with 50 samples. In the latter case, the resistances were calculated for each sample and averaged. At low voltages, single-bit errors caused significant changes in the calculated resistance, which were avoided by limiting the voltage sweep to between $0,3V$ and $2,6V$. The resistors used had a range of 0Ω , or a short-circuit, to 10Ω as this is the expected range for the gold electrodes. The results of the voltage sweep versus the multimeter test are shown in Figure 6.6.

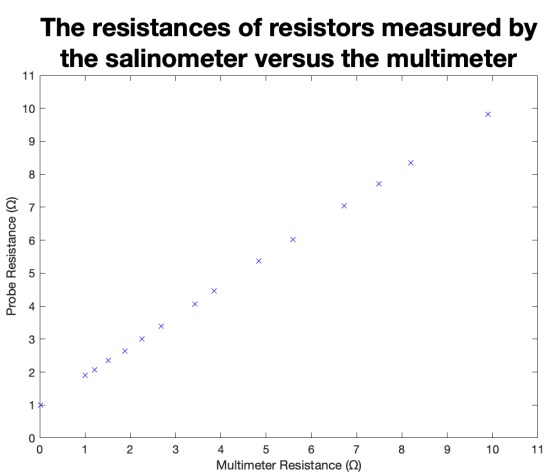


Figure 6.6: The resistance measuring test.

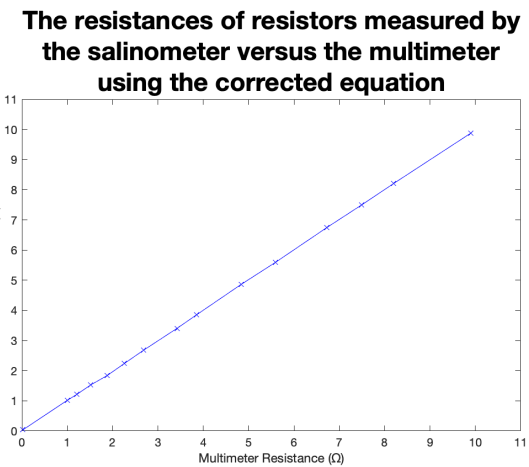


Figure 6.7: The resistance measuring test using the corrected equation.

The single voltage and voltage sweep methods were perfectly correlated with an r^2 value of 1,0000. However, there was a clear error between the probe's and the multimeter's measurements. This error

was assumed to be due to the unaccounted resistance of the switches and the traces. While these values could be measured and included in the equation, a more efficient and arguably more accurate method would be to generate an equation of best fit and use it to calculate the correct resistance.

To determine the general formula of the equation of best fit, Equation 5.1 was adjusted to include r_e , which represents the unknown resistance of the switches and traces as shown in Equation 6.1. The $R_{calibration}$, R_1 and r_e were condensed into the standard rational function coefficients p and q as shown in Equation ???. Finally, the equation was rearranged to give the electrode's resistance in terms of the measured voltage ratio as shown in Equation 6.2.

$$\begin{aligned} V_{ratio} &= \frac{\frac{R_{electrode} + r_{e1}}{R_{electrode} + R_1 + r_{e2}}}{\frac{R_{calibration} + r_{e3}}{R_{calibration} + R_1 + r_{e4}}} \\ &= \frac{R_{electrode} + r_{e1}}{R_{electrode} + R_1 + r_{e2}} \times \frac{R_{calibration} + R_1 + r_{e4}}{R_{calibration} + r_{e3}} \end{aligned} \quad (6.1)$$

$$V_{ratio} = \frac{p_1 R_{electrode} + p_2}{R_{electrode} + q_1} \quad (6.2)$$

$$R_{electrode} = \frac{p_2 - q_1 V_{ratio}}{V_{ratio} - p_1} \quad (6.3)$$

The Equation 6.2 of best fit was confirmed using MATLAB, which gave the values $p_1 = 17,4687$, $p_2 = 18,4643$ and $q_1 = 91,8315$ with an r^2 value of 1,0000. The corrected resistance values were obtained from the previous data set by reversing the previous formula and applying Equation 6.3 to the voltage ratios. These results were graphed and are shown in Figure 6.7 and have a gain of 1,0000 and an offset of 0,0000. Note that this correction equation is only valid when R_1 is 100Ω and separate equations will need to be generated should different values of R_1 be needed.

6.7 Voltage Sweep Repeatability

The following tests investigate a method for producing repeatable voltage measurements of a saltwater sample. In order to conduct these tests, the probe was cast into epoxy as described in Section 5.6.

The tests were configured with parameters such as which electrodes to use, the voltage sample count, the ADC sample count and the DAC range. Due to a circuit error discovered after the epoxy casting, the gold electrodes could only be used with the fringe guard. Thus, the effectiveness of the fringe guard was unable to be tested. Each voltage sweep produced the specified number of samples, which were transmitted over UART to a computer, where they were processed using Microsoft Excel and MATLAB to generate graphs and metrics.

The first test was a simple voltage sweep performed both forwards and in reverse with increasing and decreasing DAC voltages, respectively. The test was configured with the gold electrodes and the fringe guard, 50 voltage samples, 2 ADC samples and a voltage range of 0 – 2,6V. It was performed on a salt water sample of unknown salinity around 30 on the Practical Salinity Scale PSS-78. Ideally, the two sweeps should have been identical. However, they were not, as shown in Figure 6.8.

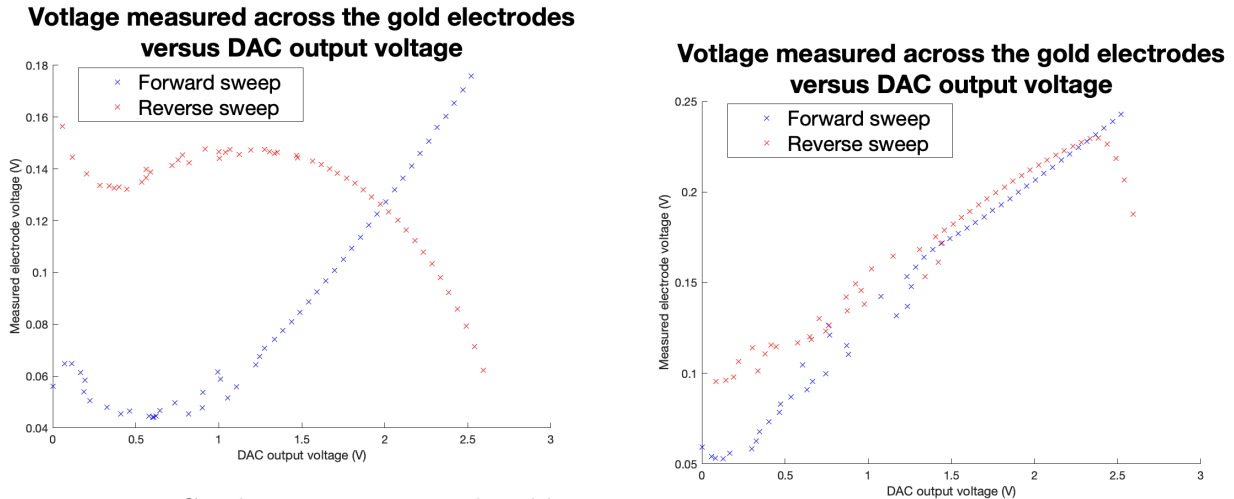


Figure 6.8: Conductivity test 1 with gold electrodes and the fringe shield, a voltage range of 0 – 2,6V, and 50 samples taken of salt water sample of unknown salinity.

Figure 6.9: Conductivity test 2 with draining and resetting the DAC between each voltage sample.

To further investigate the inconsistency, the **DAC** was drained and reset to 0V between each voltage sample before it was set to the desired voltage. It should be noted that the **DAC** drain added a slight delay between each voltage sample of around 10ms. While this did make the forward and reverse sweeps more similar, as shown in Figure 6.9, the initial voltage lag of the reverse sweep, at the higher voltages, was still present.

An alternative theory proposed that the measurements of the water briefly altered its properties, which in turn altered the proceeding measurements. This alteration was unlikely to be a capacitive effect as the measurements were taken bidirectionally, which would have dissipated any built-up charge. It was likely the voltage was dissociating the dissolved material into ions, allowing the charges in the salt water sample to move more freely [?]. However, determining exactly what was causing the alteration was beyond the scope of this project.

Instead, the theory was tested by taking priming measurements at the maximum voltage of 2,6V before capturing the actual measurements. The priming caused the actual measurements in both directions to start high and progressively move to their predicted paths, as shown in Figure 6.10.

This result supported the theory that the measurements were affecting the water. The next test varied the number of priming measurements and used 500 voltage samples to increase the curve's resolution, as shown in Figure 6.11. It should be noted that the voltage measurement effectively clipped at 0,3V as the output of the $11 \times$ gain op-amp reached $0,3 \times 11 = 3,3V$, which is the maximum voltage it can output.

While it was theoretically possible to perfectly prime a measurement, it was considered impractical, and it was also unlikely that the priming would have zero impact on the actual measurements. Thus, voltage priming was not considered a viable solution for making repeatable measurements. These results also indicated that a voltage measurement could be vulnerable to the priming effect from the previous measurement, which would cause undesirable effects. Thus, an alternative method was needed to take the measurements.

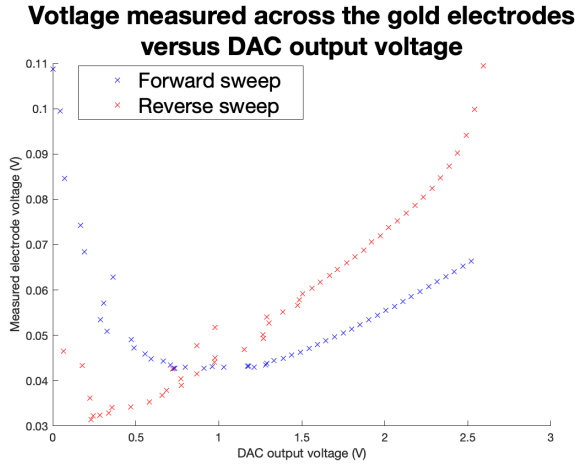


Figure 6.10: Conductivity test 3 with 25 priming measurements taken before the actual measurement.

Voltage measured across the gold electrodes versus DAC output voltage

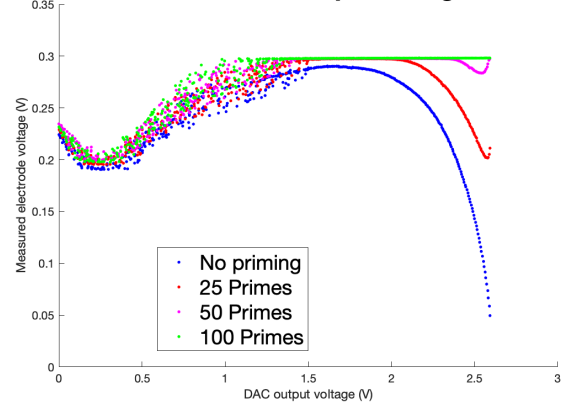


Figure 6.11: Conductivity test 4 with a varying number of priming measurements and all true measurement taken as reverse voltage sweeps with 500 voltage samples.

The priming effect decreased over time, allowing the voltage sweeps in Figure 6.10 to return to their expected curves. A new theory stemmed from this that the water could relax from a primed state over time. To test this, a delay, or relaxation time, was added between voltage samples, during which no voltage was applied to the electrodes. The first test used a relaxation time of 2s and 500ms. With a 2s relaxation time, the forward and reverse voltage sweeps were near identical, as shown in Figure 6.12. However, with a 500ms relaxation time, there was a clear difference and the same initial voltage lag shown in Figure 6.9.

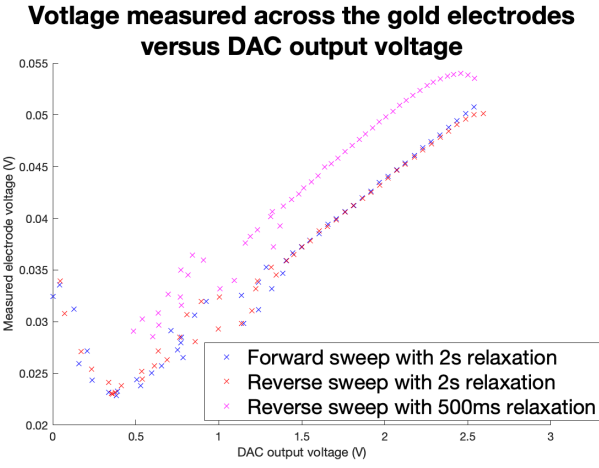


Figure 6.12: Conductivity test 5 with a varying amount of relaxation time before each measurement was taken and 50 samples.

Gold and titanium electrode ratios versus DAC output voltage

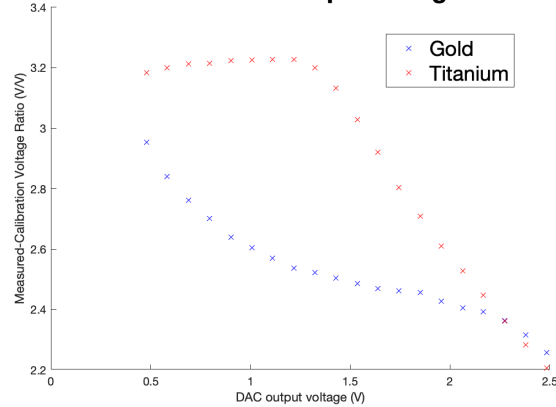


Figure 6.13: Conductivity test 6 with the difference between the titanium and gold electrodes.

This concluded a valid method of measuring a voltage sweep, which used a relaxation time of 2s between each voltage sample. This allowed the titanium electrodes to be configured. Iterative testing revealed that titanium electrodes 30mm in length spaced 6mm apart provided a good balance with an R_1 value of 100Ω . A test comparing the titanium and gold electrodes was performed, shown in Figure 6.13,

which showed that the gold electrodes followed the expected curve that Reference [38] found, while the titanium electrodes did not. The reason for this is unknown; it was theorised the fringing effect and conductivity of the titanium electrodes were the cause, which needed further investigation.

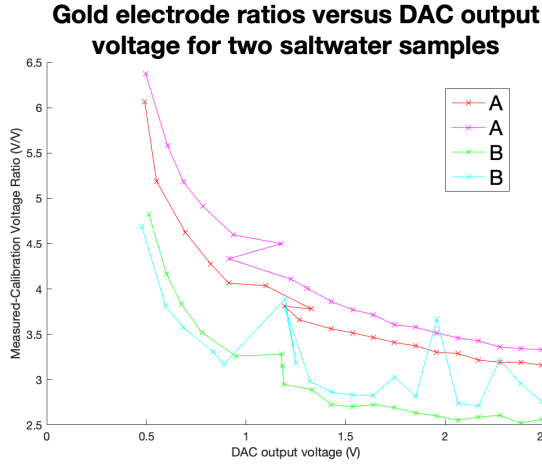


Figure 6.14: Conductivity test 7 with 4 identical tests of 20 samples with 2s of relaxation time between measurements.

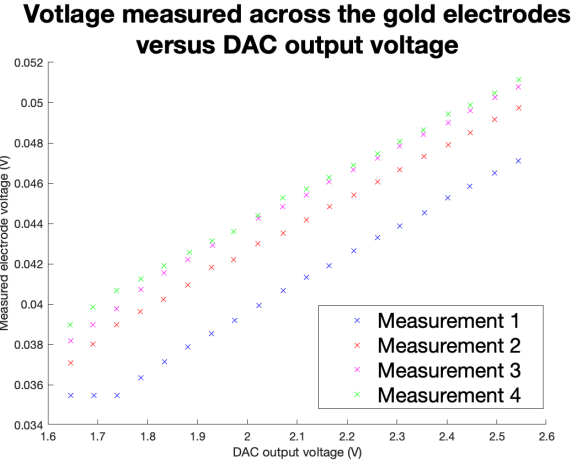


Figure 6.15: Conductivity test 6 with 4 identical tests of 20 samples with 2s of relaxation time between measurements.

The last tests to conduct for the voltage sweep were to determine the repeatability of the measurements, and to determine if there was a measurable difference between two different salt water samples. The first test took two samples of two different salt water samples with different salinities, the results of which can be seen in Figure 6.14. This showed that the voltage sweeps were approximately grouped by salinity, and there was a clear difference between the two samples. The next test aimed to prove repeatability of the measurement, taking 4 identical tests spaced shortly apart, shown in Figure 6.15. The results showed that the measurements were approximately grouped. However, it was noted that the sample's apparent conductivity was decreasing with each successive test, causing the measurements to drift upwards.

FIX. The measurement inconsistency of the voltage samples below 1,5V, shown in Figure 6.12, were present in both the electrode voltage measurement and calibration voltage measurement, and thus, were likely due to noise in either the **ADC** or op-amp. It was decided to remove this voltage range, restricting the **DAC** to between 1,65V and 2,6V, to make further data interpretation more straightforward. Similarly, the inconsistency at the end of the voltage range, shown in Figure 6.13, was likely due to the voltage lag of the reverse sweep, and thus voltages above 2V were ignored.

6.8 Voltage to Conductivity Mapping

The following tests aimed to investigate the relationship between the voltage and conductivity of a salt water sample. This required samples of known salinity, which were created by mixing sea salt and distilled water, and a handheld conductivity meter to measure the samples which was accurate to 0,1 on the Practical Salinity Scale PSS-78.

In order to correctly assess the relationship between the voltage and conductivity, the probe had to

measure a standard solution of 35 on the Practical Salinity Scale PSS-78, which was at 15°C and 0dbar . To conduct this test, the 34.8 salinity sample was placed in a fridge and cooled to below 15°C . It was then removed and 4 measurements were taken for each electrode type when the sample warmed to approximately 15°C , shown in Figure 6.16 and Figure 6.17.

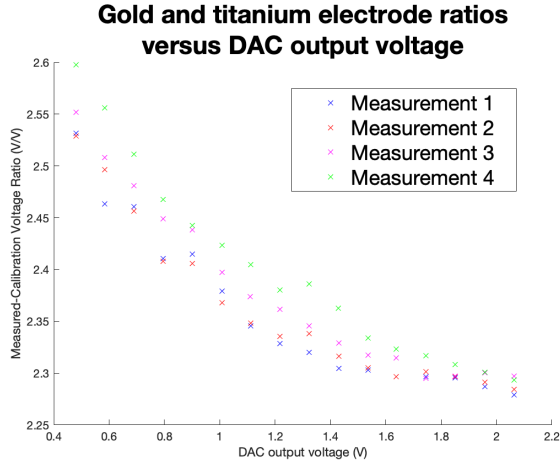


Figure 6.16: Conductivity test 6 with 4 identical tests of 20 samples with 2s of relaxation time between measurements.

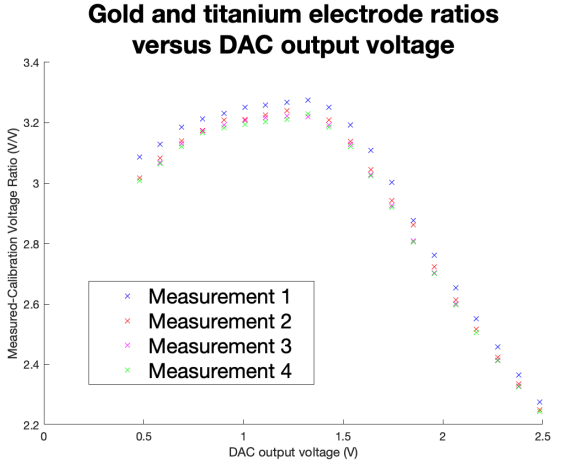


Figure 6.17: Conductivity test 7 with 4 identical tests of 20 samples with 2s of relaxation time between measurements.

The gold electrode test showed a similar discovery to the voltage sweep tests, where the measurements were grouped but increased with each successive test. The titanium electrode test showed a very different graph to the gold electrode test, appearing to have two different relationships present. The samples taken below 1.4V appeared to be concave while the samples above 1.4V appeared to be convex, following a similar curve shape to the gold electrode test. This was not due to the voltage clipping. This was theorised to be due to the fringing effect of the titanium electrodes, which was overlaying with the resistance-voltage curve of the salt water sample.

The next tests examined salt water samples of different salinities with the goal of determining if the probe could calculate the salinity from the voltage measurements. The samples were not measured at 15°C , and thus their temperature was recorded and corrected for in the calculations. The results of the 24,4 PSU sample and the 29,1 PSU sample for the gold and titanium electrodes are shown in Figure 6.18 to Figure 6.21.

These results showed a similar trend to the tests performed on the standard solution, where the measurements were grouped but increased with each successive test. The gold electrodes showed a similar trendline to the standard solution, while the titanium electrode's trendline was different below 1.4V and approximately the same above 1.4V . The titanium electrode showed remarkable consistency above 1.4V .

In order to determine salinity from the voltage sweeps, a metric was measured from each which was used in the salinity calculation. The ideal metric would be a property of the equation of best fit. The equation of best fit would logically be a hyperbolic function, where the conductivity would approach infinity as the salinity approached infinity. The equation was modified to include an offset as even with infinite conductivity, there would still be some resistance from the switches and traces in the probe. The

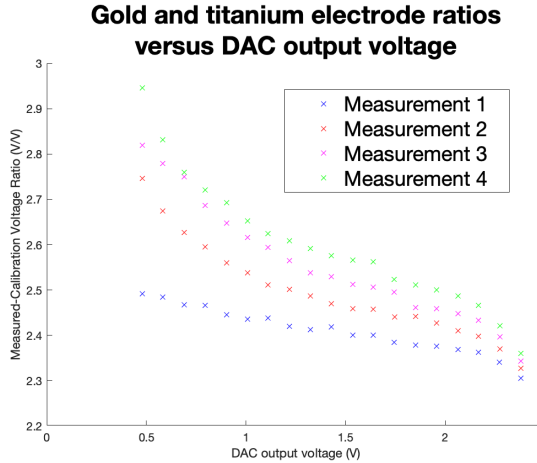


Figure 6.18: Conductivity test 6 with 4 identical tests of 20 samples with 2s of relaxation time between measurements.

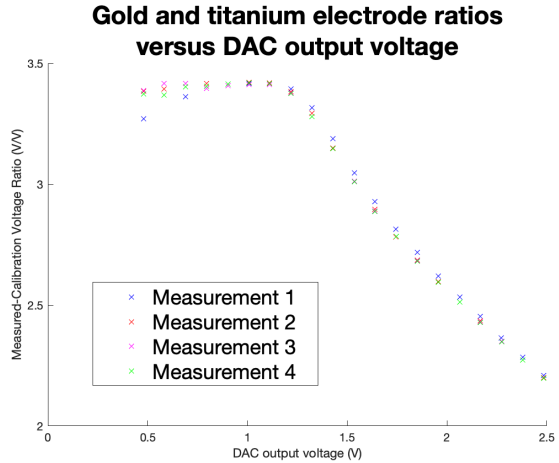


Figure 6.19: Conductivity test 7 with 4 identical tests of 20 samples with 2s of relaxation time between measurements.

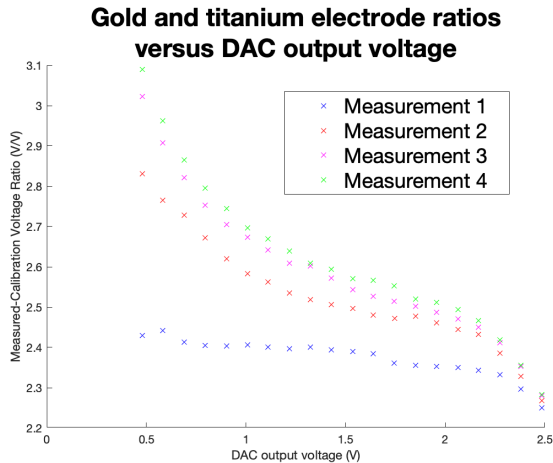


Figure 6.20: Conductivity test 6 with 4 identical tests of 20 samples with 2s of relaxation time between measurements.

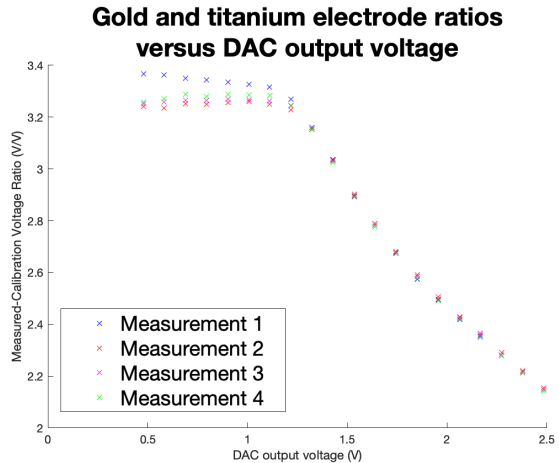


Figure 6.21: Conductivity test 7 with 4 identical tests of 20 samples with 2s of relaxation time between measurements.

equation of best fit modelled in MATLAB as $y = A/x + c$. The equation of best fit was calculated and graphed for the first sample of each saltwater sample's voltage sweep. The gold electrode removed the trailing edge, shown in Figure 6.22, and the titanium electrode removed the leading edge, shown in Figure 6.23.

This showed a logical difference between samples of similar temperature with the gold electrodes, where the lower salinity sample had a lower conductivity, equivalent to a high resistance and thus a high voltage measurement and ratio with the calibration resistor. This also showed a clear difference between samples at different temperatures. The titanium electrodes showed illogical results, where lower salinities had a lower voltage ratio. The reasons for this were unclear and would be investigated further once the gold electrodes were confirmed to be working correctly.

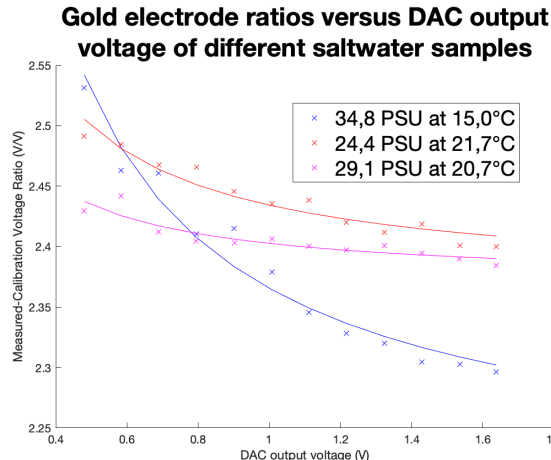


Figure 6.22: Conductivity test 6 with 4 identical tests of 20 samples with 2s of relaxation time between measurements.

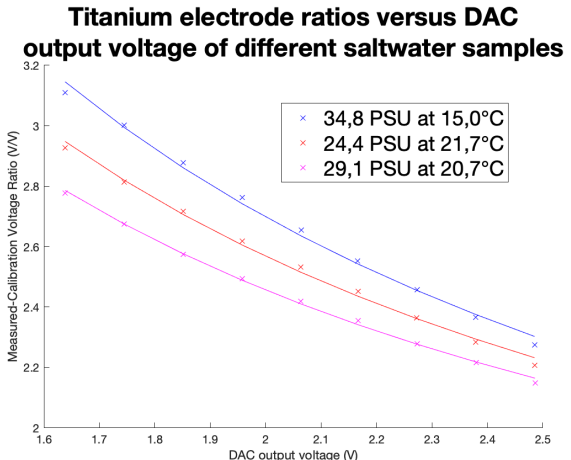


Figure 6.23: Conductivity test 7 with 4 identical tests of 20 samples with 2s of relaxation time between measurements.

6.9 Individual Voltage Measurements

Another approach that mimicked the other source was implemented which used a single voltage measurement to calculate the salinity. The voltage measurements were taken far apart from each other, to ensure that the measurements did not affect each other. The tests were conducted with the gold electrodes and the fringe guard with the **DAC** set at 1,65V, which appeared to be the most stable voltage form the previous tests. Similar to Section 6.8, a measurement of a standard solution of 34,8 **PSU** was taken, then measurements of the other three samples were taken.

The voltage ratios were adjusted to be $1/x$ to fit the hyperbolic function model, A variation using $1/x^2$, which still had the same appoximate shape, was also tested, and yielded slightly better results, which are shown in Table ??.

Table 6.2: The individual voltage measurements taken of different salt water samples.

Salinity Sample (PSU)	Voltage Ratio (V/V)	Temperature (°C)	Calculated Salinity (PSU)
34,8	2,178	15,0	-
24,4	2,320	23,7	24,9
29,1	2,288	23,7	25,5
32,9	2,058	23,7	32,2

As expected, this was not a highly accurate method of measuring salinity, but it was a good indicator of the salinity. It was able to tell the difference between the samples. However, the noise of the environment, and other slight errors affected the measurements enough to be more than a few **PSU** off.

6.10 AC Voltage Measurements

Following the approach that some CTDs and Reference [40] used, the saltwater samples were attempted to be tested using an [Alternating Current \(AC\)](#) voltage. The [AC](#) tests were performed by writing to the [DAC](#) as fast as it could operate while adding some delay, and recording the output. Measurements were taken using the [ADC](#) every time the [DAC](#) was updated. The [DAC](#) was able to produce a highly accurate sine wave which was passed through the water.

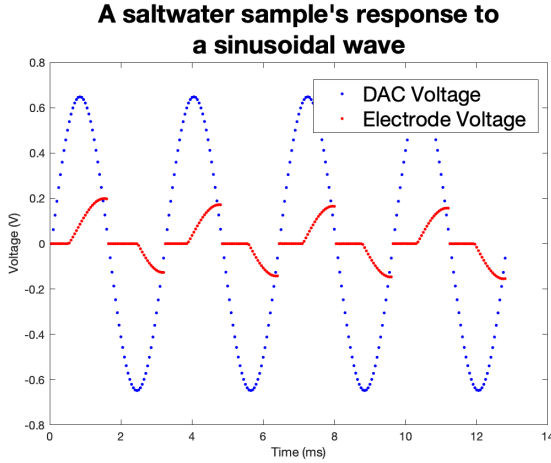


Figure 6.24: Conductivity test 6 with 4 identical tests of 20 samples with 2s of relaxation time between measurements.

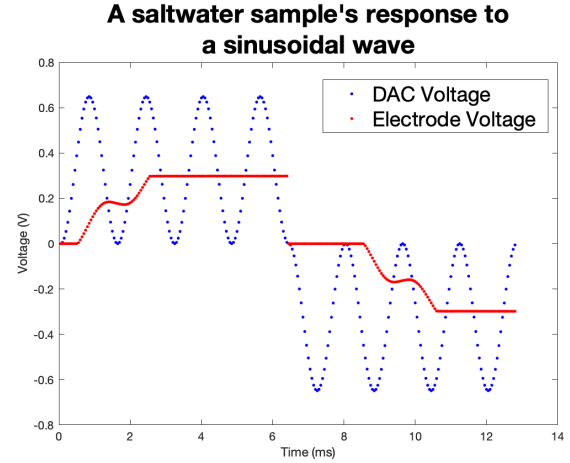


Figure 6.25: Conductivity test 7 with 4 identical tests of 20 samples with 2s of relaxation time between measurements.

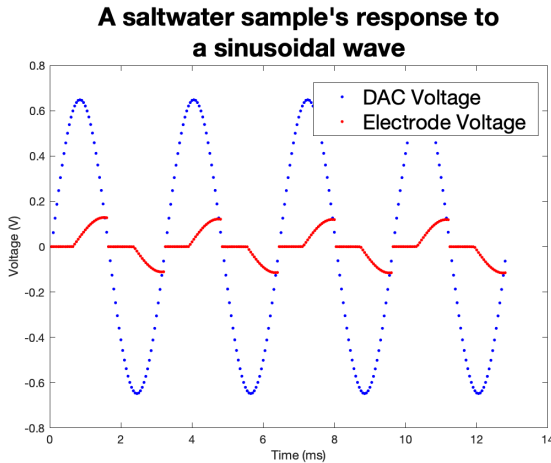


Figure 6.26: Conductivity test 6 with 4 identical tests of 20 samples with 2s of relaxation time between measurements.

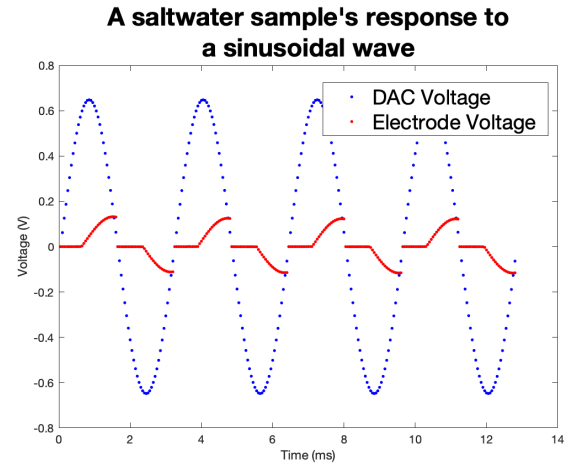


Figure 6.27: Conductivity test 7 with 4 identical tests of 20 samples with 2s of relaxation time between measurements.

Chapter 7

Conclusions

The purpose of this project was to...

This report began with...

The literature review was followed in Chapter...

The bulk of the work for this project followed next, in Chapter...

In Chapter...

Finally, Chapter... attempted to...

In summary, the project achieved the goals that were set out, by designing and demonstrating...

Chapter 8

Recommendations

probes go out the bottom and double padded.

Bibliography

- [1] National Snow and Ice Data Center, “Ice sheet quick facts,” 2024.
- [2] National Snow and Ice Data Center, “Ice shelves,” 2024.
- [3] National Oceanic and Atmospheric Administration Ocean Explorer, “Arctic exploration 2002,” 2002.
- [4] NASA Earth Observatory, “Antarctic sea ice,” 2021.
- [5] A. E. Hogg, L. Gilbert, A. Shepherd, A. S. Muir, and M. McMillan, “Extending the record of antarctic ice shelf thickness change, from 1992 to 2017,” *Advances in Space Research*, vol. 68, no. 2, pp. 724–731, 2021. 25 Years of Progress in Radar Altimetry.
- [6] R. H. Stewart, *Introduction to Physical Oceanography*. Texas A&M University Press, 2004.
- [7] R. F. HU Sverdrup, MW Johnson, *The Oceans, Their Physics, Chemistry, and General Biology*. New York: Prentice-Hall, 1942.
- [8] E. L. Lewis and R. G. Perkin, “Salinity: Its definition and calculation,” *Journal of Geophysical Research*, vol. 83, no. C1, pp. 466–478, 1978.
- [9] Y. Zheng, Y. Liu, J. Zhou, and Y. Wang, “Electrical conductivity of the global ocean,” *Earth, Planets and Space*, vol. 69, no. 1, pp. 1–10, 2017.
- [10] Sea-Bird Scientific, “What are the differences between salinity expressions in ppt, psu (practical salinity), and absolute salinity?,” 2024.
- [11] International Oceanographic Commission, “Teos-10: The international thermodynamic equation of seawater (teos-10) for temperature, salinity, density, sound speed, and other oceanographic variables,” *Manuals and Guides*, vol. 56, 2010.
- [12] Seabird Scientific, “How accurate is salinity measured by my ctd? what factors impact accuracy.”
- [13] F. J. Millero and A. Poisson, “International one-atmosphere equation of state of seawater,” *Deep Sea Research Part A. Oceanographic Research Papers*, vol. 28, no. 6, pp. 625–629, 1981.
- [14] S. Yueh, R. West, W. Wilson, F. Li, E. Njoku, and Y. Rahmat-Samii, “Error sources and feasibility for microwave remote sensing of ocean surface salinity,” *IEEE Transactions on Geoscience and Remote Sensing*, vol. 39, no. 5, pp. 1049–1060, 2001.
- [15] D. Malardé, Z. Y. Wu, P. Gross, J.-L. de Bougrenet de la Tocnaye, and M. L. Menn, “High-resolution and compact refractometer for salinity measurements,” *Measurement Science and Technology*, vol. 20, p. 015204, dec 2008.

- [16] S. Yang, J. Xu, L. Ji, Q. Sun, M. Zhang, S. Zhao, and C. Wu, “In situ measurement of deep-sea salinity using optical salinometer based on michelson interferometer,” *Journal of Marine Science and Engineering*, vol. 12, no. 9, 2024.
- [17] R. H. Byrne and F. T. Mackenzie, “Seawater,” *Encyclopædia Britannica*, 2024.
- [18] W. S. Wooster, A. J. Lee, and G. Dietrich, “Redefinition of salinity,” *Journal of Marine Research*, vol. 27, no. 3, 1969.
- [19] U.S. Geological Survey, “Water density,” 2018.
- [20] B. Kjerfve, “Measurement and analysis of water current, temperature, salinity, and density,” in *Estuarine hydrography and sedimentation* (K. Dyer, ed.), pp. 187–226, Cambridge: Cambridge University Press, 1983.
- [21] University of Washington Department of Oceanography, “A compilation of articles reporting research,” 1966.
- [22] H. Schmidt, S. Seitz, E. Hassel, and H. Wolf, “The density–salinity relation of standard seawater,” *Ocean Science*, vol. 14, no. 1, pp. 15–40, 2018.
- [23] C. T. Swift and R. E. McIntosh, “Considerations for microwave remote sensing of ocean-surface salinity,” *IEEE Transactions on Geoscience and Remote Sensing*, vol. GE-21, no. 4, pp. 480–491, 1983.
- [24] C. Gabarró, J. Font, A. Camps, M. Vall-llossera, and A. Julià, “A new empirical model of sea surface microwave emissivity for salinity remote sensing,” *Geophysical Research Letters*, vol. 31, no. 1, 2004.
- [25] The European Space Agency, “Mapping salty waters,” 2019.
- [26] R. Millard and G. Seaver, “An index of refraction algorithm for seawater over temperature, pressure, salinity, density, and wavelength,” *Deep Sea Research Part A. Oceanographic Research Papers*, vol. 37, no. 12, pp. 1909–1926, 1990.
- [27] O. A. Tengesdal, “Measurement of seawater refractive index and salinity by means of optical refraction,” Master’s thesis, University of Bergen, 2012.
- [28] Y. Liao, K. Yang, and X. Shi, “Theoretical study on simultaneous measurement of seawater temperature and salinity based on dual fiber interferometers combined with nonlinear decoupling algorithm,” *Measurement*, vol. 211, p. 112596, 2023.
- [29] G. R. C. Possetti, R. C. Kamikawachi, C. L. Prevedello, M. Muller, and J. L. Fabris, “Salinity measurement in water environment with a long period grating based interferometer,” *Measurement Science and Technology*, vol. 20, p. 034003, feb 2009.
- [30] L. V. Nguyen, M. Vasiliev, and K. Alameh, “Three-wave fiber fabry–pérot interferometer for simultaneous measurement of temperature and water salinity of seawater,” *IEEE Photonics Technology Letters*, vol. 23, no. 7, pp. 450–452, 2011.

- [31] Y. Zhao, J. Zhao, Y. Peng, R.-J. Tong, and L. Cai, "Simultaneous measurement of seawater salinity and temperature with composite fiber-optic interferometer," *IEEE Transactions on Instrumentation and Measurement*, vol. 71, pp. 1–8, 2022.
- [32] R. Somaraju and J. Trumpf, "Frequency, temperature and salinity variation of the permittivity of seawater," *IEEE Transactions on Antennas and Propagation*, vol. 54, no. 11, pp. 3441–3448, 2006.
- [33] B. Waltrip, S. Avramov-Zamurovic, and A. Koffman, "Inductance measurement using an lcr meter and a current transformer interface," in *2005 IEEE Instrumentationand Measurement Technology Conference Proceedings*, vol. 2, pp. 1005–1007, 2005.
- [34] K. A. Alhassoon, Y. Malallah, and A. S. Daryoush, "Complex permittivity and permeability extraction of ferromagnetic materials for magnetically tuned microwave circuits," *IEEE Journal of Microwaves*, vol. 1, no. 2, pp. 639–645, 2021.
- [35] P. Pattakos, A. Katsoulas, S. Angelopoulos, A. Ktena, P. Tsarabaris, and E. Hristoforou, "Development of an autonomous magnetic permeability sensor," *IEEE Transactions on Magnetics*, vol. 59, no. 2, pp. 1–4, 2023.
- [36] J. A. Ewing, "A magnetic balance for workshop tests of permeability," *Journal of the Institution of Electrical Engineers*, vol. 27, July 1898.
- [37] O. A. Tengesdal, B. L. Hauge, and L. E. Helseth, "Electromagnetic and optical methods for measurements of salt concentration of water," *Journal of Electromagnetic Analysis and Applications*, vol. 6, no. 6, 2014.
- [38] R. Benjankar and R. Kafle, "Salt concentration measurement using re-usable electric conductivity-based sensors," *Water Air and Soil Pollution*, vol. 232, no. 13, p. 13, 2021.
- [39] "Water salinity-meter : 7 steps."
- [40] J. Jonsson, K. Smedfors, L. Nyholm, and G. Thornell, "Towards chip-based salinity measurements for small submersibles and biologgers," *International Journal of Oceanography*, vol. 2013, p. 11, 2013.
- [41] Sea-Bird Scientific, "Conversion of pressure to depth," 2024.
- [42] T. L. Hill, *An introduction to statistical thermodynamics*. Courier Corporation, 1986.
- [43] A. Poisson and M. H. Gadhoumi, "An extension of the practical salinity scale 1978 and the equation of state 1980 to high salinities," *Deep Sea Research Part I: Oceanographic Research Papers*, vol. 40, no. 8, pp. 1689–1698, 1993.
- [44] G. T. Furukawa, J. L. Riddle, and W. R. Bigge, "The international practical temperature scale of 1968 in the region 13.81 k to 90.188 k as maintained at the national bureau of standards," *Journal of Research of the National Bureau of Standards-A. Physics and Chemistry*, vol. 77A, no. 3, pp. 309–322, 1973.
- [45] H. Preston-Thomas, "The international temperature scale of 1990 (its-90)," *Metrologia*, vol. 27, no. 107, pp. 3–10, 1990.

- [46] M. Solomentsev and A. J. Hanson, “Modeling current distribution within conductors and between parallel conductors in high-frequency magnetics,” *IEEE Open Journal of Power Electronics*, vol. 3, pp. 635–650, 2022.
- [47] S. Hwang and J. Shim, “A method for current spreading analysis and electrode pattern design in light-emitting diodes,” *IEEE Transactions on Electron Devices*, vol. 55, no. 5, pp. 1123–1128, 2008.
- [48] S.-R. Jeon, Y.-H. Song, H.-J. Jang, G. M. Yang, S. W. Hwang, and S. J. Son, “Lateral current spreading in GaN-based light-emitting diodes utilizing tunnel contact junctions,” *Applied Physics Letters*, vol. 78, pp. 3265–3267, 05 2001.
- [49] Jason, “Current spreading in long objects,” tech. rep., The MITRE Corporation, 7515 Colshire Drive, McLean, Virginia 22102-753, oct 2008. Approved for public release; distribution unlimited.
- [50] “What is the typical water conductivity range? | atlas scientific,” 2022.
- [51] F. Walsh, “Electrode reactions in metal finishing,” *Transactions of the Institute of Metal Finishing*, vol. 69, pp. 107–111, 08 1991.
- [52] W. J. McComas and A. K. Bhattacharya, *Inquiry into Physics*. Pearson Prentice Hall, 6th ed., 2005.
- [53] M. Hegg and A. Maminshev, “Influence of variable plate separation on fringing electric fields in parallel-plate capacitors,” in *Conference Record of the 2004 IEEE International Symposium on Electrical Insulation*, pp. 384–387, 2004.
- [54] G. J. Sloggett, N. G. Barton, and S. J. Spencer, “Fringing fields in disc capacitors,” *Journal of Physics A: Mathematical and General*, vol. 19, p. 2725, oct 1986.
- [55] Pozzebon and Alessandro, “Bringing near field communication under water: short range data exchange in fresh and salt water,” in *2015 International EURASIP Workshop on RFID Technology (EURFID)*, pp. 152–156, 2015.
- [56] N. W. Bergmann, J. Juergens, L. Hou, Y. Wang, and J. Trevathan, “Wireless underwater power and data transfer,” in *38th Annual IEEE Conference on Local Computer Networks - Workshops*, pp. 104–107, 2013.
- [57] Epoxy Technology, “Understanding how to choose an appropriate thermally conductive epoxy.”
- [58] Total Materia, “Joining titanium,” 2005.